Differential GABAergic and glycinergic inputs of inhibitory interneurons and purkinje cells to principal cells of the cerebellar nuclei

Husson, Zoé ; Rousseau, Charly V ; Broll, Ilja ; Zeilhofer, Hanns Ulrich ; Dieudonné, Stéphane

Abstract: The principal neurons of the cerebellar nuclei (CN), the sole output of the olivo-cerebellar system, receive a massive inhibitory input from Purkinje cells (PCs) of the cerebellar cortex. Morphological evidence suggests that CN principal cells are also contacted by inhibitory interneurons, but the properties of this connection are unknown. Using transgenic, tracing, and immunohistochemical approaches in mice, we show that CN interneurons form a large heterogeneous population with GABA/glycinergic phenotypes, distinct from GABAergic olive-projecting neurons. CN interneurons are found to contact principal output neurons, via glycine receptor (GlyR)-enriched synapses, virtually devoid of the main GABA receptor (GABAR) subunits 1 and 2. Those clusters account for 5% of the total number of inhibitory receptor clusters on principal neurons. Brief optogenetic stimulations of CN interneurons, through selective expression of channelrhodopsin 2 after viral-mediated transfection of the flexed gene in GlyT2-Cre transgenic mice, evoked fast IPSCs in principal cells. GlyR activation accounted for 15% of interneuron IPSC amplitude, while the remaining current was mediated by activation of GABAR. Surprisingly, small GlyR clusters were also found at PC synapses onto principal CN neurons in addition to 1 and 2 GABAR subunits. However, GlyR activation was found to account for <3% of the PC inhibitory synaptic currents evoked by electrical stimulation. This work establishes CN glycinergic neurons as a significant source of inhibition to CN principal cells, forming contacts molecularly distinct from, but functionally similar to, Purkinje cell synapses. Their impact on CN output, motor learning, and motor execution deserves further investigation.

DOI: https://doi.org/10.1523/JNEUROSCI.0401-14.2014

Cellular/Molecular

Differential GABAergic and Glycinergic Inputs of Inhibitory Interneurons and Purkinje Cells to Principal Cells of the Cerebellar Nuclei

Zoé Husson,[1] Charly V. Rousseau,[1] Ilja Broll,[2] Hanns Ulrich Zeilhofer,[3] and Stéphane Dieudonné[1]

[1]Ecole Normale Supérieure, Institut de Biologie de l'ENS (IBENS), Inserm U1024, and CNRS UMR 8197, F-75005 Paris, France, [2]Institute of Pharmacology and Toxicology, University of Zurich, CH-8057 Zürich, Switzerland, and [3]Institute of Pharmaceutical Sciences, Swiss Federal Institute of Technology (ETH Zürich), CH-8090 Zürich, Switzerland

The principal neurons of the cerebellar nuclei (CN), the sole output of the olivo-cerebellar system, receive a massive inhibitory input from Purkinje cells (PCs) of the cerebellar cortex. Morphological evidence suggests that CN principal cells are also contacted by inhibitory interneurons, but the properties of this connection are unknown. Using transgenic, tracing, and immunohistochemical approaches in mice, we show that CN interneurons form a large heterogeneous population with GABA/glycinergic phenotypes, distinct from GABAergic olive-projecting neurons. CN interneurons are found to contact principal output neurons, via glycine receptor (GlyR)-enriched synapses, virtually devoid of the main GABA receptor (GABAR) subunits α1 and γ2. Those clusters account for 5% of the total number of inhibitory receptor clusters on principal neurons. Brief optogenetic stimulations of CN interneurons, through selective expression of channelrhodopsin 2 after viral-mediated transfection of the flexed gene in GlyT2-Cre transgenic mice, evoked fast IPSCs in principal cells. GlyR activation accounted for 15% of interneuron IPSC amplitude, while the remaining current was mediated by activation of GABAR. Surprisingly, small GlyR clusters were also found at PC synapses onto principal CN neurons in addition to α1 and γ2 GABAR subunits. However, GlyR activation was found to account for $<$3% of the PC inhibitory synaptic currents evoked by electrical stimulation. This work establishes CN glycinergic neurons as a significant source of inhibition to CN principal cells, forming contacts molecularly distinct from, but functionally similar to, Purkinje cell synapses. Their impact on CN output, motor learning, and motor execution deserves further investigation.

Key words: **cerebellar nuclei; glycinergic; immunohistochemistry; interneurons; mixed inhibition; optogenetics**

Introduction

The cerebellar nuclei (CN) form the sole output of the cerebellar system integrating direct pathways and indirect pathways via the cerebellar cortex. Important components of cerebellar plasticity (Zheng and Raman, 2010) and sensorimotor learning (Miles and Lisberger, 1981; Medina et al., 2000) are implemented in the CN rather than in the cerebellar cortex, although the latter was more extensively studied. Hence, understanding information processing in the CN, including how local connectivity controls the activity of CN principal cells (Uusisaari and Knöpfel, 2012) is a central endeavor for cerebellar studies.

The CN contain different types of projection neurons: output neurons such as glutamatergic principal cells projecting to premotor structures or glycine-containing large neurons of the medial nucleus projecting to brainstem nuclei (Wassef et al., 1986; Bagnall et al., 2009), small GABAergic neurons mediating the nucleo-olivary feedback loop (Fredette and Mugnaini, 1991; De Zeeuw et al., 1997), and nucleo-cortical neurons (Houck and Person, 2014). Purkinje cells (PCs) of the cerebellar cortex provide a massive GABAergic projection to all these neuronal types (De Zeeuw and Berrebi, 1995; Teune et al., 1998; Uusisaari and Knöpfel, 2008), thereby controlling the output of the CN (Ito et al., 1970; Chen et al., 2010; Hoebeek et al., 2010; Person and Raman, 2012a; Chaumont et al., 2013).

The persistence of GABAergic synapses in the CN of PC-degeneration (PCD) mutant mice (Wassef et al., 1986) provided the first evidence for a source of CN inhibition different from

Received Jan. 29, 2014; revised May 16, 2014; accepted June 7, 2014.

Author contributions: Z.H. and S.D. designed research; Z.H. and C.V.R. performed research; I.B. and H.U.Z. contributed unpublished reagents/analytic tools; Z.H. and C.V.R. analyzed data; Z.H. and S.D. wrote the paper.

Research was supported by CNRS, INSERM, and ENS (École Normale Supérieure), and by Agence Nationale de la Recherche (ANR) Grants INNET (BL2011) and Cecomod (MNP2009) to S.D. and by the Advanced Investigator ERC (European Research Council) Grant (DHISP, 250128) to H.U.Z. This work has received support under the program "Investissements d'Avenir" launched by the French Government and implemented by the ANR (ANR-10-LABX-54 MEMO LIFE; ANR-11-IDEX-0001-02 PSL* Research University). Z.H. is a recipient of a fellowship from Université Pierre et Marie Curie–ED3C. C.V.R. received a fellowship from Fondation pour la Recherche Médicale (FRM). We thank Dr. P. Isope for making available the L7-ChR2-YFP transgenic mice; Dr. A. Dumoulin for α1-GlyR antibodies and useful advice on glycine immunostaining; Dr. M. Diana for his help with stereotaxic injections and viruses; Dr. M. Spolidoro for her help with retrobead injections; Dr. R. Proville for help and advice on GNU R and analysis; B. Mathieu for his help at the IBENS imaging platform financed by FRM, Region Ile de France, FRC, and France Bio-Imaging; and Dr. B. Barbour and Dr. C. Léna for careful reading of the manuscript and helpful discussions.

The authors declare no competing financial interests.

Correspondence should be addressed to Stéphane Dieudonné, IBENS, S4.9, 46 rue d'Ulm, F-75005 Paris, France. E-mail: dieudon@biologie.ens.fr.

C. V. Rousseau's present address: Division of Neurophysiology, MRC National Institute for Medical Research, The Ridgeway, Mill Hill, London NW7 1AA, UK.

DOI:10.1523/JNEUROSCI.0401-14.2014

 0270-6474/14/349418-14$15.00/0

PCs. Early morphological studies had identified a population of small CN neurons with local axonal arborization (Matsushita and Iwahori, 1971; McCrea et al., 1978). The glycine immunoreactivity of many small somata in the CN (Rampon et al., 1996; Bäurle and Grüsser-Cornehls, 1997; Zeilhofer et al., 2005) and the abundance of glycinergic synapses in the CN of wild-type animals (Chen and Hillman, 1993; De Zeeuw and Berrebi, 1995) and PCD mutants (Bäurle and Grüsser-Cornehls, 1997) established the inhibitory nature of these local neurons. These glycinergic interneurons differ from glycine/aspartate projection neurons by size and electrophysiological properties (Bäurle and Grüsser-Cornehls, 1997; Uusisaari et al., 2007; Uusisaari and Knöpfel, 2010). Glycinergic interneurons thus constitute a separate neuronal class of the CN, but their functional impact in a structure massively innervated by GABAergic inputs from PCs remains to be clarified.

Glycine receptors (GlyRs) are expressed in the CN (Malosio et al., 1991; Pedroarena and Kamphausen, 2008) and inhibitory chloride currents have been evoked by glycine application in principal cells of young rats (Kawa, 2003; Pedroarena and Kamphausen, 2008). Small isolated strychnine-sensitive synaptic currents have been also evoked in principal cells by pharmacological or ionic manipulations of the CN (Kawa, 2003; Pedroarena and Kamphausen, 2008). However, further evidence for functional glycinergic inhibition provided by CN interneurons is still lacking.

Using immunohistochemical and optogenetic approaches, we show here that interneurons provide a significant inhibitory input to CN principal neurons through mixed GABAergic/glycinergic synapses displaying distinctive molecular components. These data argue for a role of glycinergic interneurons, together with PCs, in controlling the output of the CN.

Materials and Methods

Animals

Adult (3- to 5-month-old) *GlyT2-eGFP* transgenic mice (Zeilhofer et al., 2005) were used to perform immunostaining. Heterozygous *GlyT2-Cre* (kind gift from H. U. Zeilhofer, University of Zurich, Zurich, Switzerland) male mice were bred with either homozygous *Rosa26-Floxed-mTmG* or *Rosa26-Floxed-mTmT* female mice, and Cre-positive offspring (2–3 months old) were used for immunostaining. *GlyT2-Cre* heterozygous transgenic adult mice were also used for stereotaxic injections of adeno-associated viruses (AAVs). For optogenetic experiments, injections were performed at P30 and recordings were performed at P50–P55. For GlyT2 immunostaining, adult *GlyT2-Cre* mice (10–11 months old) were injected with the virus and processed 1 month later. Adult *Thy1-ChR2-YFP* mice (15 months old, line 18; Wang et al., 2007) and *L7-CHR2-YFP* mice (3–4 months old; Chaumont et al., 2013) were used for immunostaining. Heterozygous *Thy1-CFP* animals (aged P30–P60; Feng et al., 2000) were used to patch principal cells in electrophysiological experiments. Either males or females were used in all experiments. All animal manipulations were made in accordance with guidelines of the Centre National de la Recherche Scientifique.

Stereotaxic injections

GlyT2-Cre mice (1 month old for electrophysiological experiments, 10–11 months old for immunostaining experiments) were deeply anesthetized with ketamine-xylazine (106 mg/kg and 7.5 mg/kg, respectively) and placed in a stereotaxic frame. Two holes were made in the skull above the right and left CN. A pulled quartz capillary (35–40 μm tip diameter) was lowered into the brain at the proper coordinates, and 500 μl of viral constructs AAV2.1.EF1α.DIO.hChR2(H134R).eYFP (plasmid from K. Deisseroth, Stanford University, Stanford, CA; Kravitz et al., 2010; virus from Laboratoire de Thérapie Génique—UMR 649, Nantes, France) was slowly pressure-injected at each site at the rate of one 30 ms pulse every 5 s, with a pressure of 30 psi (Picospritzer II, General Valve Corporation). Animals were closely monitored for 3 d until recovery from surgery and then housed for 3–4 weeks. Animals were then killed for acute slice experiments as described below.

Adult *GlyT2-eGFP* animals (3–5 months old) were injected in the inferior olive, with 10–50 nl of Retrograde Beads (Red RetroBeads, Lumafluor) from a dorsal entry point.

Immunohistochemistry

Tissue fixation, preparation, and labeling for GABA receptor-GlyR immunostaining. Animals were deeply anesthetized with an intraperitoneal injection of sodium pentobarbital (50 mg/kg) and perfused through the aorta with an ice-cold solution of 1× PBS (Sigma) followed by 50–75 ml of 4% w/v paraformaldehyde (PAF; VWR International) dissolved in 1× PBS, pH 7.4. The entire brain was then dissected and kept in 4% PAF at 4°C overnight. Samples were then rinsed and embedded in paraffin (Leica). Slices of 7 μm thickness were cut with a microtome, mounted on SuperFrost Ultra Plus slides (Thermo Fisher Scientific), and treated for antigen retrieval as previously described (Rousseau et al., 2012). For immunohistochemistry, mounted sections were incubated overnight at 4°C with the following primary antibodies: chicken GFP antibody at 1:1000 final dilution (Avès), mouse pan-GlyR (mAB4a) antibody at 1:1000 final dilution (Synaptic Systems), rabbit α1-GlyR (kind gift from Andrea Dumoulin; Machado et al., 2011), rabbit γ2-GABAR (GABA receptor)antibody at 1:1500 final dilution (Synaptic Systems), rabbit α1-GABAR antibody at 1:500 final dilution (Synaptic Systems), guinea pig GlyT2 antibody at 1:1500 final dilution (Millipore Bioscience Research Reagents), guinea pig VIAAT (vesicular inhibitory amino acid transporter) antibody at 1:1500 final dilution (Synaptic Systems), mouse VGluT2 antibody at 1:1500 final dilution (Millipore). Tissue sections were rinsed with PBS and then incubated with secondary antibodies coupled to 488, 549, or 649 DyLight fluorophores (Jackson ImmunoResearch) or Alexa Fluor 555 IgG (Invitrogen) at room temperature during 2 h at 1:500 final dilution. Slices were mounted in Prolong Gold Antifade Reagent (Sigma).

Tissue fixation and preparation for GABA immunostaining. Animals were deeply anesthetized by intraperitoneal injection of sodium pentobarbital (50 mg/kg). Tracheotomy was performed before opening the rib cage, and assisted-ventilation with medical oxygen was maintained during intra-aortic perfusion with an oxygenated (95% O_2-5% CO_2) ice-cold solution of 1× PBS followed by 4% PAF dissolved in 1× PBS, pH 7.4. The brain was dissected and kept overnight in 4% PAF solution at 4°C.

Free-floating immunostaining for GABA and GAD65–67 labeling. After perfusions of the animals and postfixations overnight of the brains in 4% PAF dissolved in 1× PBS, pH 7.4, brains were cryoprotected by equilibration in 30% sucrose w/v-PBS at 4°C and then cut on a cryomicrotome (−20°C, 30–60 μm thickness). Free-floating sections were washed twice for 10 min in PBS and permeabilized for 2 h at room temperature in PBS-0.4% v/v Triton X-100. Nonspecific sites were saturated by incubation in PBS-0.4% Triton X-100–1.5% cold fish skin gelatin at room temperature for 3 h. Primary antibodies were applied overnight at 4°C in a PBS solution containing 0.1% Triton X-100–1.5% fish gelatin (mouse GABA antibody mAB 3A12, Swant, final dilution 1:10,000; mouse GAD65–67 antibody mAB 9A6, Enzo Life Sciences, final dilution 1:500). After three washes of 30 min in PBS-0.1% Triton X-100, slices were incubated overnight at 4°C with secondary antibodies diluted in PBS-0.1% Triton X-100–1.5% cold fish skin gelatin. Slices were finally rinsed with PBS 3 times for 30 min each and mounted in either Fluoromount (Sigma) or Mowiol solution (made from powder, Fluka-Sigma).

Image acquisition and analysis

Acquisition and deconvolution. Image stacks were acquired using an inverted confocal microscope (Leica SP5) at 60 × 60 × 170 nm voxel size, using a 63× oil-immersion objective. For image deconvolution, point-spread functions (PSFs) were measured for each wavelength on subresolution (175 nm) fluorescent beads (PS-Speck, Invitrogen) embedded in 7.5% w/v porcine gelatin in 1× PBS, and mounted in Prolong Gold Antifade Reagent (Sigma). Bead images were extracted from image stacks using a custom routine in ImageJ (W. S. Rasband, ImageJ, U.S. National

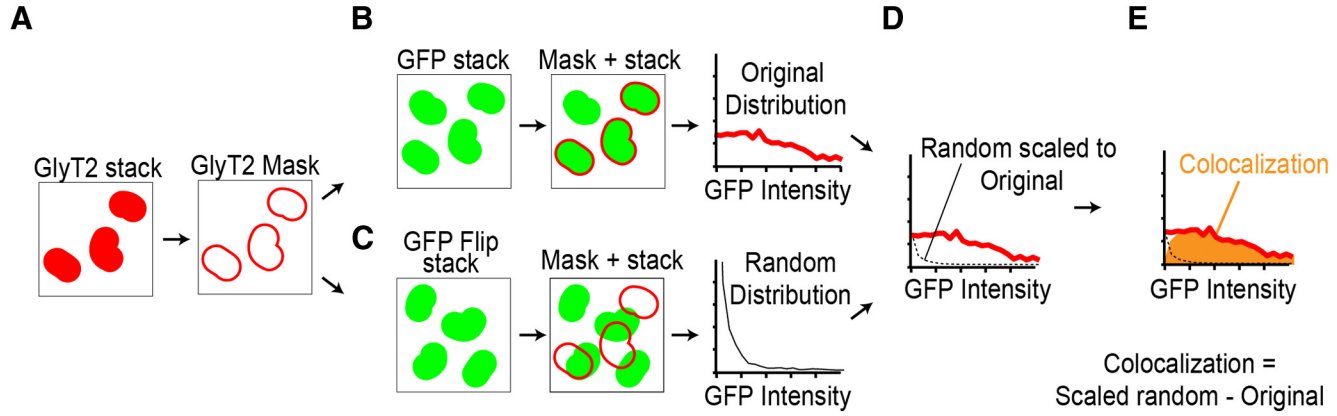

Figure 1. Method for colocalization quantification in confocal *Z*-stacks. ***A***, To quantify the colocalization rate between two markers, for example GlyT2 (red fluorescence signal) over GFP varicosities (green fluorescence signal), GlyT2+ varicosities are detected in stacks and converted as a binary mask. ***B***, ***C***, This mask is used to retrieve mean GFP intensities below each immunoreactive aggregate in the original GFP stack (***B***, original distribution in solid red line) and in a flipped GFP stack (***C***, random distribution in black solid line). ***D***, This latter distribution is scaled to the original distribution (black dashed line). ***E***, The difference between the original distribution and the scaled randomized distribution provides an underestimate of true colocalization (orange).

Institutes of Health, Bethesda, MD, http://imagej.nih.gov/ij/, 1997–2012) and averaged to obtain an experimental PSF. Selected image stacks were then deconvolved using a custom routine based on preexisting ImageJ plugins Iterative Deconvolve 3D (Dougherty, 2005, http://www.optinav.com/imagej.html) and Objet Counter 3D (Bolte and Cordelières, 2006; http://rsbweb.nih.gov/ij/plugins/track/objects.html). Results were then further processed using GNU R ("R: A Language and Environment for Statistical Computing," R Core Team, R Foundation for Statistical Computing, Vienna, Austria, 2013, http://www.R-project.org) and custom routines.

Cluster detection and quantification. Five to 10 optical slices were sequentially averaged (800–1700 nm *Z* projection) along the whole stack and clusters of receptors were detected on the resulting pictures as ROIs using a threshold-based method. ROI statistics (number of pixels, mean intensity, and total intensity) were then retrieved for each ROI on individual color channels (GlyR and GABAR). Using GNU R, we computed the fraction of labeling intensity attributable to one of the channels for each ROI.

Colocalization analysis. To assess colocalization between two markers, we designed a custom routine using Fiji (Schindelin et al., 2012) and GNU R (Fig. 1). Mean intensities of marker 1 beneath each ROI detected for marker 2 (as previously described; Fig. 1*A*) were collected in the original stack of marker 1 and plotted (Fig. 1*B*, red solid lines). To estimate the noise and nonspecific colocalization, mean intensities of marker 1 were also collected in a randomized marker 1 stack (horizontally and vertically flipped; Fig. 1*C*, black solid line). In the random distribution, the first bins in the initial peak represent ROI with barely undetectable mean intensities and could be considered as noncolocalized elements, whereas the tail of the distribution is considered to be "by-chance" colocalized ROI. Noncolocalized elements would be found in the first low-intensity bins of the original distribution, but it is impossible to draw a clear line between colocalized elements on a low-intensity view of marker 1 and noncolocalized elements. Our parti-pris was to systematically underestimate colocalization by assuming that noncolocalized elements in the original distribution had the same bimodal distribution as the random distribution. We obtained the underestimated colocalization (Fig. 1*E*, in orange) by scaling the randomized distribution to the original distribution (Fig. 1*D*, black dashed lines), using the average amplitude of the first bins ($n = 3$ in each case) of the histograms and subtracting this scaled random distribution from the original distribution. This custom routine was used to assess rate of colocalization between GlyT2 and GFP markers in different transgenic mice, and between Thy1-YFP and GlyR- and GABAR-enriched clusters. In the case of YFP staining in Thy1-ChR2-YFP mice, YFP intensities of *Z*-projected sections of the stacks were first scaled according to the slope of the fit to the logarithmic distribution of their pixel intensity. The "subtract background" ImageJ plugin was then applied.

Apposition analysis. Apposition analysis was performed in 3D using Imaris 7.2 software (Bitplane). Clusters and varicosities (either VIAAT-positive or GlyT2-positive) were detected, and distances between the cluster centers and the closest varicosity surface were retrieved in original and randomized stacks (one channel horizontally and vertically flipped).

Statistical analysis. Statistical analysis was performed using GNU R and Igor Pro (Wavemetrics). Results are represented as mean ± SD unless otherwise specified. Statistical tests were performed using nonparametric Wilcoxon rank-sum and signed-rank tests and significance was assumed if $p \leq 0.05$.

Electrophysiology

Slice preparation. Animals were sedated with isoflurane (4% in medical oxygen) and deeply anesthetized with ketamine-xylazine (106 mg/kg, 7.5 mg/kg) before being perfused with two consecutive iced protective, oxygenated (95% O_2-5% CO_2) solutions [in distilled water; Solution 1 (in mM): 115 NaCl, 26 $NaHCO_3$, 3 KCl, 0.8 $CaCl_2$, 8 $MgCl_2$, 1.25 NaH_2PO_4, 25 glucose, 1 lidocaine, 1 ketamine; Solution 2: 230 sucrose, 26 $NaHCO_3$, 3 KCl, 0.8 $CaCl_2$, 8 $MgCl_2$, 1.25 NaH_2PO_4, 25 glucose, 1 lidocaine, 1 ketamine; Isope and Barbour, 2002]. Animals were then decapitated and the cerebellum was rapidly removed from the skull. The cerebellum was glued (Cyanolit) in the slicing chamber on its anterior face and submerged in ice-cold cutting solution [in Volvic Water, containing the following (in mM): 130 K-gluconate, 14.6 KCl, 2 EGTA, 20 HEPES, 25 glucose, 50 10-3 D-APV, 50 10-6 minocycline] during slicing. Slices (290 μm thickness) were cut using a ceramic blade (*Z* deflection < 0.5 μm) with an oscillating blade microtome (Campden Instruments) and kept in warm (33°C) oxygenated recovery solution [in Volvic Water (containing, in mM): 225 D-mannitol, 2.3 KCl, 1.25 NaH_2PO_4, 25 $NaHCO_3$, 25 glucose, 0.51 $CaCl_2$, 7.7 $MgCl_2$, 50 10-3 D-APV, 50 10-6 minocycline] during several minutes before being transferred to a chamber recirculated with warm (33°C) oxygenated BBS solution [in Volvic Water (containing, in mM): 125.7 NaCl, 3.3 KCl, 1.25 NaH_2PO_4, 24.8 $NaHCO_3$, 25 glucose, 1.3 $CaCl_2$, 1.17 $MgCl_2$, 50 10-6 minocycline].

Electrophysiological recordings. At least 30 min after being cut, slices were transferred to a recording chamber mounted on an Olympus BX51WI microscope equipped with an epifluorescence illumination pathway and a CoolSnap camera (Roper Scientific, Photometrics). Slices were perfused with warm gassed BBS solution (3.5 ml/min, at 33°C). Borosilicate glass patch electrodes (resistance 3–4.5 MΩ) were filled with a high-Cl^- intracellular solution containing the following (in mM): 105 CsCl, 20 TEA-Cl, 10 HEPES, 10 QX314, 10 EGTA, 1 $CaCl_2$, 5 $MgCl_2$, 4 ATP-Na, 0.4 GTP-Na, pH adjusted to 7.4 with CsOH (290–295 mOsm). Recordings were made in the interposed and lateral nuclei to avoid larger glycinergic projection neurons in the medial nucleus (Bagnall et al., 2009). Whole-cell patch-clamp recordings were performed using a HEKA EPC10 amplifier and PatchMaster acquisition software (HEKA).

Cells were held at −70 mV in the whole-cell configuration and electrophysiological signals were digitized at a sampling rate of 20 kHz. A Bessel filter at 5 kHz was used.

Electrical and optical stimulations. Electrical stimulations of PC axons were performed a few hundred micrometers from the recorded cell in the white matter surrounding the CN, using a Master-9 stimulator (Isoflex Stimulus Isolation Unit, A.M.P.I.). Using regular patch pipettes (3–5 MΩ), bipolar stimulation intensities in the 20–90 V range (200 μs) were necessary to evoke a stable response in the recorded cells. Optogenetic stimulations of GlyT2-positive CN neurons were achieved with 470 nm LED illumination (Thorlabs) of 1 ms duration with a power density of 0.3–4 mW/mm^2 (measured under the objective lens). Drugs were bath-applied, and a delay of 5–6 min after addition of the drug was always respected to allow for complete diffusion into the slice.

Drugs. All electrophysiological experiments were performed in the presence of 50 μM D-APV (Abcam) and 10 μM NBQX (Abcam) to block NMDA and AMPA receptors. In some experiments, strychnine (Abcam) and SR 95531 (gabazine, Abcam) were added to the bath.

Data analysis. Electrophysiological data were analyzed with Igor Pro 6.1 (Wavemetrics). Statistical analysis was performed using R GNU. Between 250 and 400 sweeps were averaged for each condition. All data are presented as mean ± SD. For statistical significance, Wilcoxon rank-sum and signed-rank tests were used, as applicable.

Analysis of pharmacological data

To estimate the maximum possible contribution of GlyR to the synaptic currents, gabazine and strychnine were considered to exert independent, nonsynergistic, antagonist effects on GABAR and GlyR. Gabazine fractional block (G) of the GABAR response at a concentration of 300 nM was obtained by applying gabazine in the presence of 1 μM strychnine. In our calculations, strychnine was considered to block 100% of the GlyR current (Jonas et al., 1998). Let us call Y the fraction of the IPSC amplitude mediated by GlyR and U the unspecific fractional block of GABAR by strychnine (corrections can be performed either for 300 nM or 1 μM strychnine). Then the fractional block of the IPSC by strychnine alone is $Y + U * (1 - Y)$ and the fractional block of the control response by strychnine after 300 nM gabazine is $[Y + U * G * (1 - Y)]$. Solving these two equations yields Y and U.

Results

Identification of glycinergic interneurons in the CN

We sought to identify the inhibitory interneurons of the CN by their glycinergic phenotype using two transgenic mouse models based on the promoter of the neuronal plasma membrane glycine transporter GlyT2, a specific marker of glycinergic neurons (Zafra et al., 1995). In the first model the eGFP was placed directly under the control of the GlyT2 promoter (*GlyT2-eGFP* mice, Fig. 2*A*; Zeilhofer et al., 2005), whereas in the second (*GlyT2-Cre* mice) the Cre recombinase was placed under the control of the GlyT2 promoter. To reveal Cre expression, GlyT2-Cre mice were bred with *R26-loxed-mTmG* reporter mice in which lox-directed switchable Tomato and GFP are placed under the control of the ubiquitous neuronal promoter *Rosa 26* (Muzumdar et al., 2007; Fig. 2*B*).

A large number of small GFP+ neurons, putative interneurons, were seen in all subdivisions of the CN in both models and a few large GFP+ projection neurons were seen in the medial nucleus (Fig. 2*A*,*B*). In addition to GFP+ cell bodies, all the CN were densely populated by GFP+ neurites, which in many instances could be traced back to small GFP+ cell bodies (Fig. 2*C*). Coimmunostaining against VIAAT (VGAT), a ubiquitous marker of inhibitory axonal varicosities, identified the majority of these neurites as axons and confirmed the interneuronal nature of small GlyT2-eGFP-positive cells in the CN (Fig. 2*Ca*). Axons presented clear VIAAT-immunoreactive varicosities (Fig. 2*Cb*, solid arrows) separated by thin profiles of uniform diameter. Dendrites may also be thin and contorted, but they present more irregular VIAAT-immunonegative profiles (Fig. 2*Cb*, dashed arrows).

Number of glycinergic neurons in the CN

To estimate the number and density of glycinergic neurons in the CN, fluorescent cell bodies were counted in complete serial sections of *GlyT2-Cre* × *R26-loxed-mTmT mouse* CN ($n = 3$ animals) and *GlyT2-eGFP* mice ($n = 3$ animals). The number of positive neurons was estimated to 2007 ± 367 and 627 ± 37 in the interposed nuclei of the *GlyT2-Cre* × *R26-loxed-mTmT* and *GlyT2-eGFP* mice, respectively, and to 2132 ± 567 and 643 ± 68 in the lateral nucleus (cells were not counted in the medial nucleus because large projecting glycinergic neurons were also found in this area). In these two nuclei the density of positive neurons was 5560 ± 1708 neurons/mm^3 in *GlyT2-Cre* × *R26-loxed-mTmT* mice and 1561 ± 32 neurons/mm^3 in *GlyT2-eGFP* mice. The large difference of neuron count between the two models suggests either that a fraction of glycinergic neurons do not express GFP in the *GlyT2-eGFP* mouse line or that the expression is not restricted to glycinergic neurons in *GlyT2-Cre* mice, due to developmental leakage of Cre recombinase expression.

To compare the specificity of our two genetic models, we performed immunostaining against the membrane transporter GlyT2 (Fig. 2*D*,*E*). GlyT2+ varicosities and axonal profiles were abundant in all nuclei. GlyT2+ varicosities were detected using a threshold-based method, and the rate of GlyT2-GFP colocalization was assessed using a procedure detailed in Figure 1 (see Materials and Methods), which will be used repeatedly in this article (Fig. 2*F*,*G*). In the *GlyT2-eGFP* mouse, the rate of colocalization of GlyT2 over GFP was only 40% (Fig. 2*D*,*F*), confirming the mosaic expression in this transgenic line. In contrast, >89% of the GlyT2+ varicosities displayed GFP staining in *GlyT2-Cre* × *R26-loxed-mTmG* offspring (Fig. 2*E*,*G*). Hence, most if not all glycinergic interneurons of the CN express the Cre recombinase at one stage of their development in *GlyT2-Cre* mice and are stained by GFP in adult *GlyT2-Cre* × *R26-loxed-mTmG* offspring. Applying a correction factor of 2.5 for the mosaic expression in the *GlyT2-eGFP* models yields an estimate of the total number of glycinergic neurons of 1567 in the interposed nuclei and 1607 in the lateral nuclei, for an estimated density of 3900 neurons/mm^3. This was still much lower than in the *GlyT2-Cre* × *R26-loxed-mTmT* mice, suggesting the occurrence of nonspecific expression in this genetic background.

Closer examination of the *GlyT2-Cre* × *R26-loxed-mTmT* mice revealed fluorescence expression in some PCs mainly located in the vermis and projecting to the medial nucleus. Furthermore, expression was found in a large number of small cell bodies located in the ventral part of the CN and resembling the morphology of inhibitory neurons projecting to the inferior olive (nucleo-olivary cells; Fig. 2*Ha*). A specific expression in nucleo-olivary neurons was further confirmed by the observation of numerous fluorescent axons invading the dorsal olive (Fig. 2*Hb*). Both small neurons concentrated in the ventral part of the CN (Fig. 2*Ia*), and axons in the olive (Fig. 2*Ib*) were absent from the *GlyT2-eGFP* animals. When Flexed AAVs were injected into the CN of 1-month-old *GlyT2-Cre* animals, the pattern of expression was similar to the pattern found in *GlyT2-GFP* mice both for the cell density in the CN (the absence of small cells in the ventral CN) and for the absence of fibers in the olive. We conclude that the nonspecific pattern of expression observed in the *GlyT2-Cre* × *R26-loxed-mTmT* crossings is due to the temporary developmental expression of the Cre recombinase in all glycinergic CN

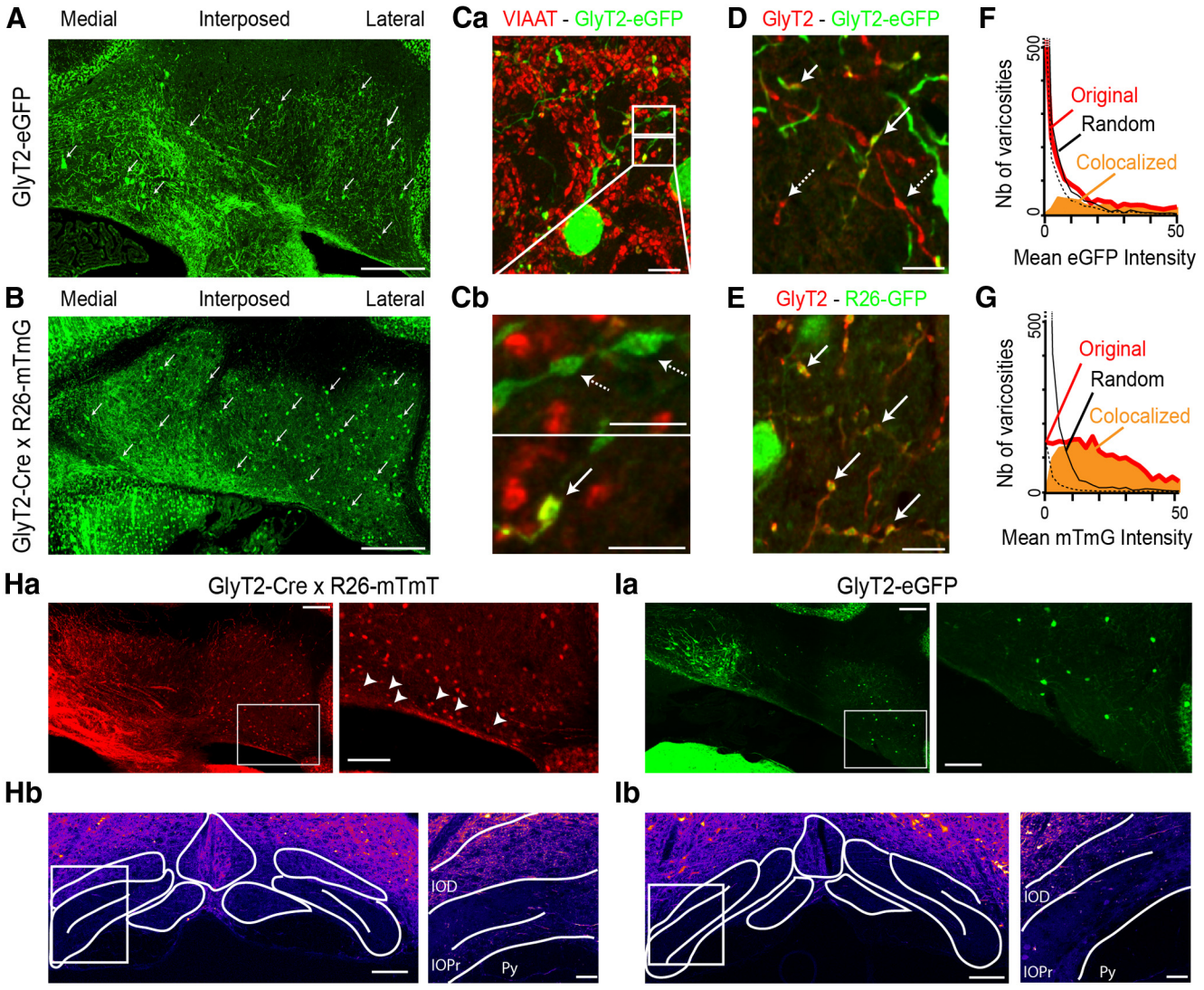

Figure 2. Transgenic mice as tools to study glycinergic interneurons in cerebellar nuclei. ***A***, Coronal slice of the CN in the *GlyT2-eGFP* mouse. Arrows indicate GlyT2-eGFP+ cells within the three cerebellar nuclei (medial, interposed, and lateral nuclei). ***B***, Coronal slice of cerebellar nuclei (medial, interposed, and lateral) in a *GlyT2-Cre* × *Rosa26-loxed-mTmG* mouse. Note the abundance of GFP+ cells (solid arrows) compared with the *GlyT2-eGFP* mouse. ***Ca***, ***Cb***, Costaining of GlyT2-eGFP+ neurons with VIAAT (red) allows distinguishing between local axonal varicosities (solid arrows) and VIAAT-immunonegative dendrites (dashed arrows). *Z*-thickness of projection: ***Ca***, 8.8 μm; ***Cb***, 2 μm. ***D***, GlyT2 costaining of the *GlyT2-eGFP* mouse reveals that only a fraction of GlyT2+ profiles colocalize with GFP (solid arrows), whereas a majority do not colocalize (dashed arrows). *Z*-thickness of projection, 1.7 μm. ***E***, Near-complete colocalization is found in the *GlyT2-Cre* × *Rosa26-loxed-mTmG* mouse. *Z*-thickness of projection, 1.7 μm. ***F***, In the *GlyT2-eGFP* mouse, distribution histograms of GFP intensities under GlyT2+ profiles (red) and spatially randomized profile distribution (black; see Materials and Methods and Fig. 1) yield an estimate of colocalization of GlyT2+ profiles with GFP-positive profiles of 40% (orange area). ***G***, In the *Rosa26-loxed-mTmG* × *GlyT2-Cre* mouse, at least 89% of GlyT2+ varicosities were colocalized with GFP+ profiles. ***H***, Inferior olive coronal sections in the *GlyT2-Cre* × *Rosa26-loxed-mTmT* mouse. ***Ha***, In the cerebellar nuclei of the *GlyT2-Cre* × *Rosa26-loxed-mTmT* mouse, small nucleo-olivary cells are stained and are particularly visible in the ventral part of the nuclei (solid arrowheads). ***Hb***, Faint labeling of the axons of nucleo-olivary cells is visible in the inferior olive of the *GlyT2-Cre* × *Rosa26-loxed-mTmT* mouse, particularly in the dorsal subnucleus (*Z*-thickness of projection, 32 μm). ***I***, In the *GlyT2-eGFP* mouse, the nucleo-olivary neuron somata were not visible in the cerebellar nuclei (***Ia***), while virtually no axonal projections were seen in the inferior olive (***Ib***). *Z*-thickness of projection, 32 μm. Scale bars: ***A***, ***B***, ***Ha***, ***Hb***, ***Ia***, ***Ib***, 200 μm; ***Ca***, ***D***, ***E***, 10 μm; ***Cb***, 5 μm; ***Ia***, ***Ib*** inset, 100 μm; ***Ha***, ***Hb*** inset, 50 μm. IOD, Dorsal nucleus of inferior olive; IOPr, principal nucleus of inferior olive, Py, pyramidal tract.

neurons but also in some Purkinje cells and nucleo-olivary neurons. Because of this lack of specificity, the *GlyT2-eGFP* mouse was exclusively used for further morphological studies, keeping in mind that only ~40% of the glycinergic interneurons are eGFP+ in this genetic background.

Glycinergic neurons in the CN are distinct from nucleo-olivary cells

To confirm that the GFP+ neurons found in the *GlyT2-eGFP* mice and the small nucleo-olivary neurons constitute separate populations of cells, injections of retrograde fluorescent beads were performed in the inferior olive of GlyT2-eGFP mice ($n = 3$ animals; Fig. 3*A*). Retrolabeled cells found in the CN were never eGFP positive (0 of 488 cells; Fig. 3*B*). However, closer examination revealed a level of fluorescence of their cell bodies slightly above background, indicative of the fact that GFP may have been expressed at earlier developmental stages. Immunostaining for GABA also differentiated glycinergic interneurons from olivary projecting cells. Retrogradely labeled cells did not stain for GABA at their somata (Fig. 3*B*), although it is well established that GABA neurotransmission occurs at their terminals in the inferior olive through unusual asynchronous release (Best and Regehr, 2009). In contrast, 38.6 ± 21.5% of the eGFP-positive neurons in the *GlyT2-eGFP* animals ($n = 3$ animals, $n = 570$ eGFP-positive

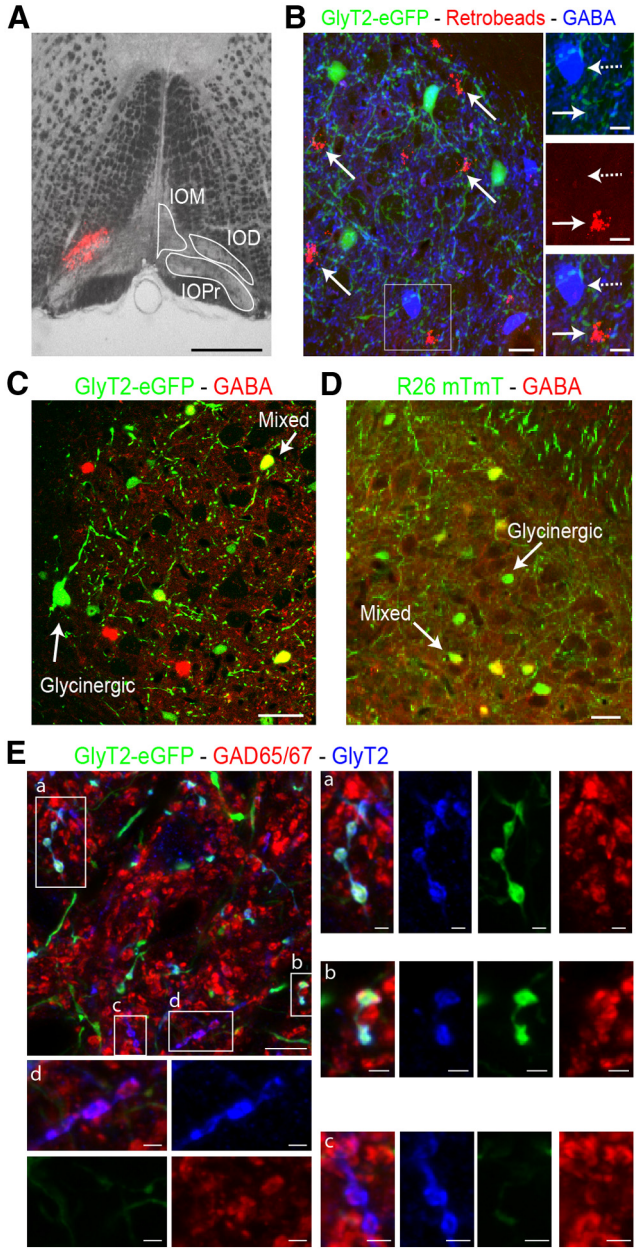

Figure 3. CN interneurons constitute a population distinct from inferior olive-projecting neurons and present mixed GABAergic-glycinergic phenotypes. ***A***, Bright-field image of a coronal slice of the inferior olive in a *GlyT2-eGFP* mouse injected with red fluorescent retrograde beads. ***B***, In the CN, retrolabeled cells (red; solid arrows) were not GlyT2-eGFP-positive (green) and do not exhibit GABA staining (blue) at their soma (see inset). *Z*-thickness of projection, 26 μm. ***C***, In the *GlyT2-eGFP* mouse, some GFP-positive neurons (green) are found costained for GABA (red). ***D***, In a *Rosa26-loxed-mTmT* × *GlyT2-Cre* mouse, all neurons stained for GABA (red) at their somata are mTmT-positive (green), whereas some mTmT-positive neurons do not show GABA staining. ***Ea–Ed***, In the *GlyT2-eGFP* mouse, the mixed GABAergic/glycinergic phenotype of most glycinergic neurons, whether eGFP positive (green) or not, is confirmed by costaining of GlyT2 axonal varicosities (blue) with GAD65–67 (red). *Z*-thickness, 1.7 μm. IOM, Medial nucleus of inferior olive; IOD, dorsal nucleus of inferior olive; IOPr, principal nucleus of inferior olive. Scale bars: ***A***, 50 μm; ***B–D***, 20 μm; ***E***, 10 μm; ***B*** inset, 10 μm; ***E*** close-ups ***a–d*** (right), 2 μm.

neurons) displayed GABA immunostaining (Fig. 3*C*). Conversely, we found that only 42.5 ± 23.4% of GABA-positive somata were stained for GFP in the *GlyT2-eGFP* mice (n = 98 GABA-positive neurons; Fig. 3*C*), in agreement with the fraction of interneurons stained in this model, whereas 89.1 ± 15.1% of GABA-positive somata also stained for mTmT in the *Rosa26-loxed-mTmT* × *GlyT2-Cre* offspring (n = 3 animals, n = 105 GABA-positive neurons; Fig. 3*D*).

As exemplified by the case of the nucleo-olivary cells, somatic staining for GABA is not a reliable marker of the GABAergic phenotype of the transmission at axonal varicosities. To evaluate the extent of GABA and glycine corelease by the CN interneurons, costaining for GlyT2 and GAD65–67 was performed in *GlyT2-eGFP* animals (Fig. 3*E*). GFP+ axonal varicosities were differentiated from dendrites by their GlyT2 staining, as previously described (Fig. 2*D*). Those varicosities, as well as GFP-negative GlyT2-positive profiles, were always colabeled for GAD65–67 (Fig. 3*E*, inset). These data argue for the accumulation and corelease of GABA and glycine at the great majority of interneuron synapses. Thus, inhibitory interneurons of the CN constitute a specific cell type, distinct from the nucleo-olivary cells, and characterized by their mixed glycinergic/GABAergic inhibitory phenotype.

Different types of inhibitory receptor clusters in the CN

To identify the postsynaptic targets of CN mixed inhibitory interneurons and assess the localization and abundance of their synapses relative to the dominant GABAergic innervation coming from PCs, we performed coimmunostaining against glycine receptor subunits (pan-GlyR mAb4a antibody) and the γ2 subunit of $GABA_A$ receptors (GABAR-γ2), which is strongly expressed in the CN (Araki et al., 1992; Fig. 4*A*). Numerous GABAR-γ2 clusters were found throughout the neuropil and covering the somata and large initial dendrites of presumptive large projection neurons (Fig. 4*A*). Surprisingly, these clusters appeared colocalized with small glycine receptor clusters. In addition, a population of somewhat larger glycine receptor clusters, which did not appear to costain for GABAR-γ2, was present in the neuropil and on the initial dendrites of principal neurons (Fig. 4*A*).

To quantify these observations, we first performed threshold-based cluster detection (Fig. 1; see Materials and Methods) on the summed GABAR-γ2 and pan-GlyR signals. Then GlyR and GABAR immunoreactivities were integrated separately under each cluster area, and the ratio GlyR/(GlyR + GABAR-γ2) staining was computed. The distribution of this ratio was bimodal, identifying GlyR-enriched and GABAR-enriched clusters (Fig. 4*B*). In some cases, low GlyR expression led to the appearance of a probably spurious peak of GABAR-only clusters (1.1 ± 0.7% of all clusters; the number of clusters in each stack varies between 1 and 47 clusters, n = 158 detected clusters, n = 7 stacks, data not shown), which were only slightly more intense than the other GABAR-enriched clusters (137.3 ± 39.80%, Wilcoxon test $p = 5.4e^{-6}$). We thus considered that GABAR-only clusters represent an extreme form of GABA-enriched clusters but cannot exclude that they constitute a rare synaptic class.

GABAR-γ2 labeling was barely detectable in GlyR-enriched clusters (6.7 ± 3.5% of the staining of GABAR-enriched clusters, n = 7 stacks, n = 1185 detected clusters; Fig. 4*C*). Furthermore, glycine receptor staining intensity in GlyR-enriched clusters was 181.3 ± 57.0% of that of GABAR-enriched clusters (minimum, 132%; maximum, 280%; Wilcoxon test, $p < 2.2e^{-16}$, n = 7 stacks; 2112 ± 547 clusters per stack). Overall, GlyR-enriched clusters represented 8.2 ± 2.5% of the total number of immunoreactive profiles (n = 7 stacks, n = 14,790 detected clusters). Similar results were reproduced with an antibody against the α1 subunit of the GABA receptor (Fig. 4*D*). In this case, the GlyR-enriched population amounted to 8.7 ± 3.3% of the total number of clusters (n = 10 stacks, n = 23,009 clusters detected; Fig. 3*E*,*F*). Finally, immunostaining against the α1 subunit of the

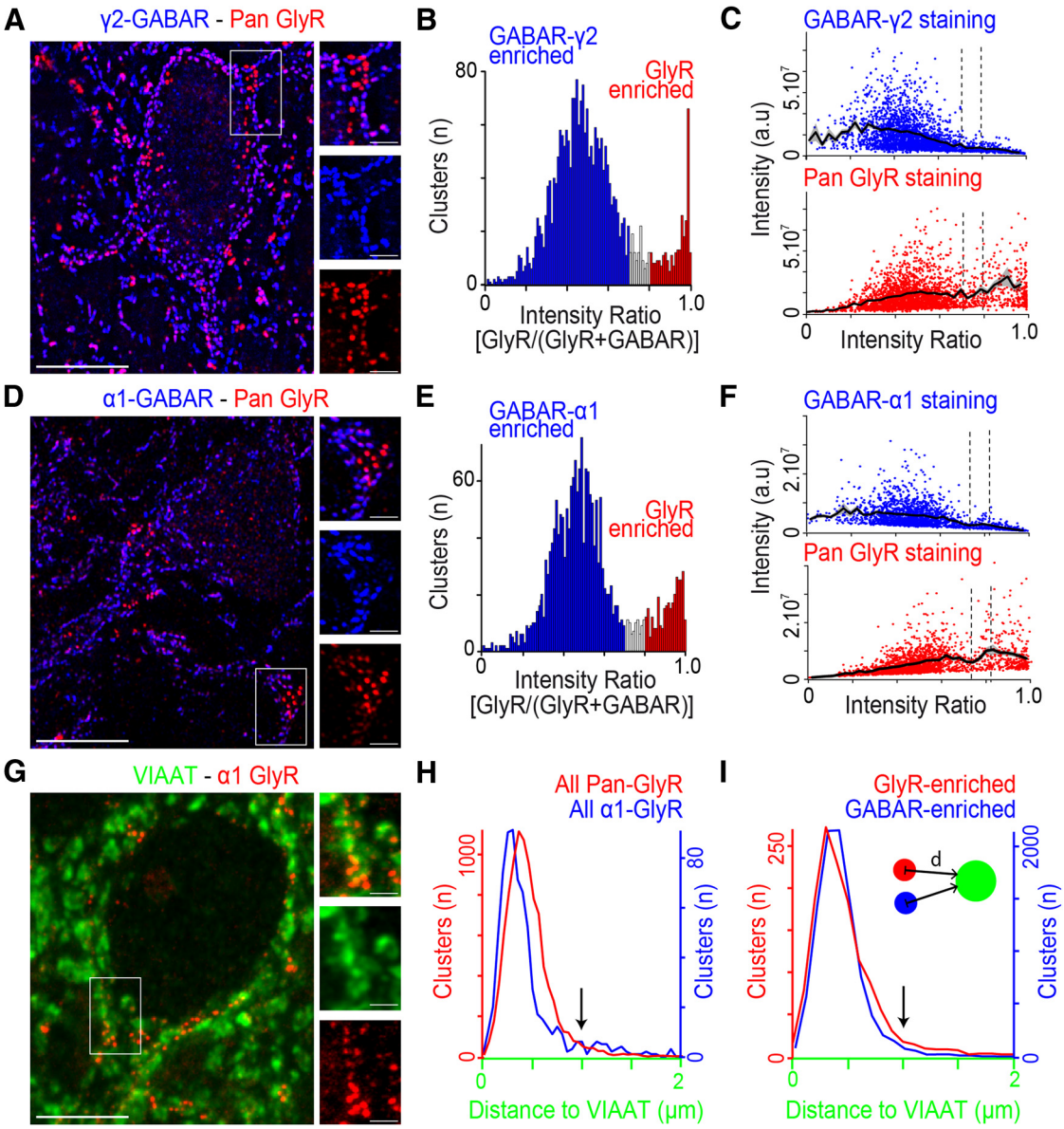

Figure 4. Different types of postsynaptic inhibitory receptor clusters in the CN. ***A***, Costaining for the γ2 subunit of GABAR (blue) and pan-GlyR subunits (red) reveals two main populations of clusters. *Z*-thickness of projection, 8 μm. ***B***, Example of intensity ratio histogram between the GlyR signal and the sum of the GlyR and GABAR signals in all clusters of one stack. The histogram exhibits a bimodal distribution that allow us to distinguish between GABAR-γ2-enriched clusters (blue bins) and GlyR-enriched clusters (red bins). ***C***, Plot of GABAR-γ2 and pan-GlyR intensities (in arbitrary units, a.u.), as a function of the intensity ratio. The smoothed average over the 2495 clusters detected is represented (black lines, mean ± SD), showing the decreasing and increasing intensity trends for GABAR-γ2 and GlyR clusters, respectively. ***D–F***, Similar observations are obtained with costaining for GABAR-α1 subunit (blue) and pan-GlyR (red; $n = 2088$ detected clusters). ***G***, GlyR α1 subunit immunoreactivity (red) is found on somata of presumptive principal CN cells and clusters are seen apposed to VIAAT-positive varicosities (green). *Z*-thickness of projection, 8 μm. ***H***, The distribution of distances reveals that the majority of both pan-GlyR (red line) and α1-GlyR (blue line) clusters are found within 1 μm from VIAAT-positives varicosities. ***I***, Similarly, both GlyR-enriched (red line) and GABAR-enriched (blue line) clusters are located within a distance of 1 μm from the VIAAT-positive element. Scale bars: ***A***, ***D***, ***G***, 10 μm; ***A***, ***D***, ***G*** close-ups (right), 2 μm.

glycine receptor revealed a very similar size and distribution of glycine receptor clusters, confirming the specificity of pan-GlyR immunostaining (Fig. 4*G*). These data demonstrate the existence of two types of postsynaptic differentiation in the CN, expressing different ratios of γ2/α1-containing GABARs and α1-containing glycine receptors, which we shall subsequently call GABAR-enriched and GlyR-enriched clusters.

GABAR-enriched and GlyR-enriched clusters are in apposition to PC terminals and glycinergic interneurons, respectively

We investigated the localization of GlyR-enriched and GABAR-enriched postsynaptic clusters relative to the inhibitory presynaptic terminals identified by immunostaining against VIAAT. The vast majority of glycine receptor clusters were found within 1 μm of VIAAT immunostaining (Fig. 4*H*), whether GlyRs were stained for α1 (85.0 ± 8.3%, $n = 8$ stacks, $n = 2299$ detected clusters) or for pan-GlyR (96.7 ± 0.5%, $n = 5$ stacks, $n = 9638$ detected clusters). This was a shorter distance than predicted in the random distribution obtained when flipping VIAAT stacks (α1-GlyR: original distribution, 0.7 ± 0.5 μm vs random distribution, 1.3 ± 1.1 μm, Wilcoxon test $p < 2.2e^{-16}$; pan-GlyR: original distribution, 0.5 ± 0.2 μm vs random distribution, 0.9 ± 0.5 μm, Wilcoxon test $p < 2.2e^{-16}$). GABAR-enriched clusters and GlyR-enriched clusters were found at similar distances from VIAAT profiles (Fig. 4*G*; GlyR-enriched

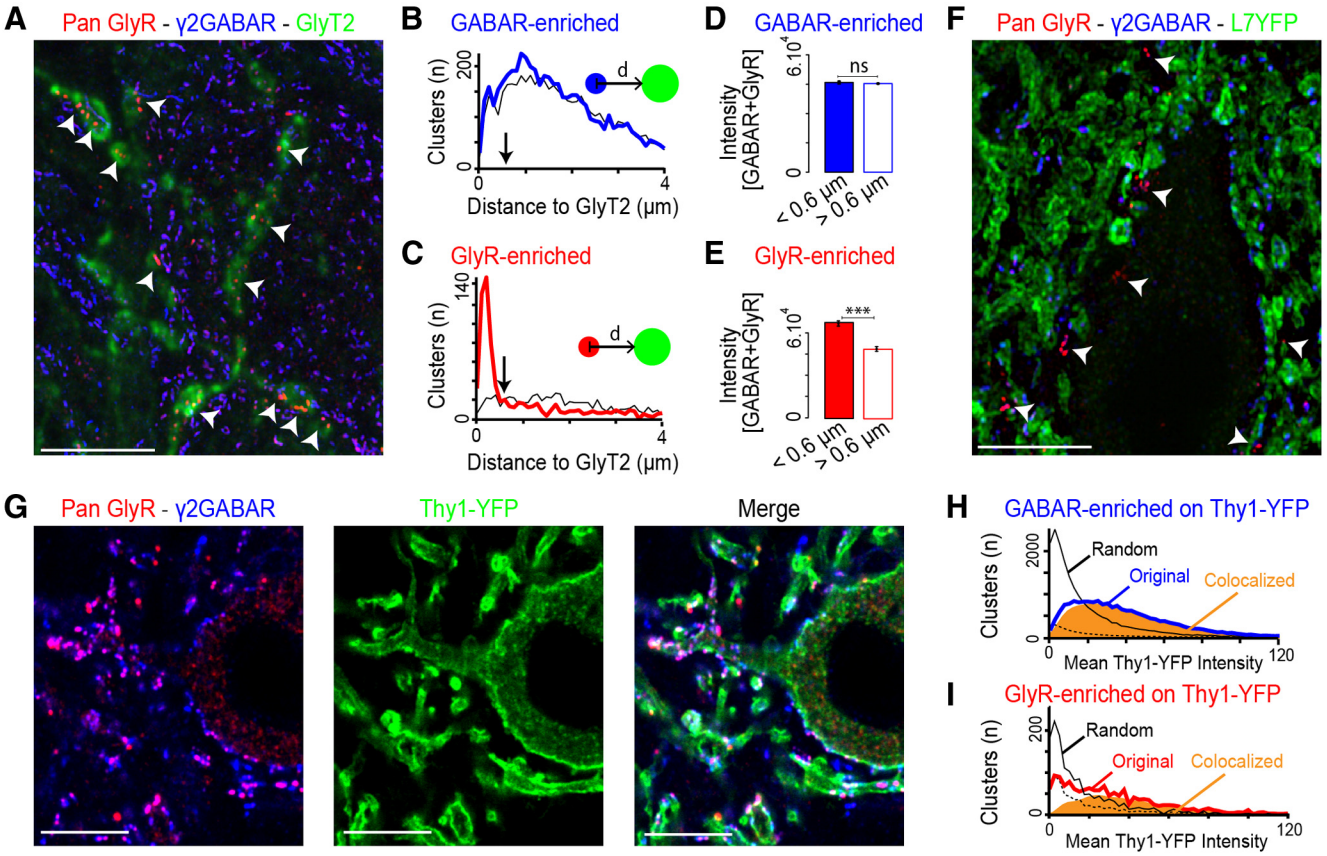

Figure 5. GABAR-enriched clusters and GlyR-enriched clusters are located on principal neurons and face Purkinje cell varicosities and GlyT2+ profiles, respectively. ***A***, GlyR-enriched clusters are found in front of GlyT2+ varicosities (white arrowheads) as shown in costaining for pan-GlyR (red), GABAR-γ2 (blue), and GlyT2 (green). *Z*-thickness of projection, 8.3 μm. ***B***, ***C***, Analysis of distance distributions to the closest GlyT2-positive varicosities (red lines) reveals that 59.3 ± 8.5% of GlyR-enriched clusters are found at <0.6 μm from a varicosity, whereas distribution of distances for GABAR-enriched clusters (blue line) was not different from randomized data (black lines). ***D***, ***E***, Nonapposed GlyR-enriched clusters have lower intensities (summed GlyR+GABAR) than apposed clusters (Wilcoxon test, $p \ll 0.01$). ***F***, Costaining for pan-GlyR (red) and GABAR-γ2 (blue) in a *L7-ChR2-YFP* (green) mouse reveals appositions between L7-positive Purkinje cell terminals and GABAR-enriched, but not GlyR-enriched, clusters (white arrowheads). *Z*-thickness of projection, 1.2 μm. ***G***, Costaining for pan-GlyR (red) and GABAR-γ2 (blue) in a *Thy1-ChR2-YFP* (green) mouse, in which CN principal cells exhibit YFP staining at the membrane. *Z*-thickness of projection, 0.51 μm. ***H***, ***I***, Colocalization analysis as previously described (Fig. 2*E*) reveals that >88% of GABAR-γ2-enriched clusters and >59% for GlyR-enriched clusters are colocalized with YFP, indicating that they are located on principal cells. Scale bars: ***A***, ***B***, ***G***, 10 μm.

clusters, 0.46 ± 0.21 μm; GABAR-enriched clusters, 0.49 ± 0.26 μm), indicating that both types of receptor aggregates are postsynaptic to inhibitory varicosities.

We sought for the identity of presynaptic elements facing the two types of receptor clusters. We used triple staining against pan-GlyR, GABAR-γ2, and GlyT2 (Fig. 5*A*) to study the spatial relationship between glycinergic terminals from local interneurons and GlyR-enriched clusters. Receptor clusters were detected and GlyT2+ profiles were segmented in 3D (Imaris software; see Materials and Methods). The distance between each cluster center and the closest surface of a GlyT2+ profile was calculated using original and flipped GlyT2 stacks, to control for nonspecific appositions (Fig. 4*B*,*C*). The distribution of the distances between GABAR-enriched clusters and GlyT2+ varicosities did not show a peak for small values and was similar to the randomized distribution (Fig. 5*B*). In contrast, the distance distribution of GlyR-enriched clusters showed a marked peak for short distance, and 59.3 ± 8.5% of GlyR-enriched clusters were found within 0.6 μm of a GlyT2+ varicosity (Fig. 5*C*), significantly more than expected at random (12.8 ± 4.7%; Wilcoxon test, $p < 2.2e^{-16}$). Those appositions were also found in the *GlyT2-eGFP* mouse (data not shown), but only 27.9 ± 20.9% of GlyR-enriched clusters were found within 0.6 μm of a GlyT2-eGFP+ varicosity, in agreement with the observed mosaic expression in this transgenic line. Hence, the most likely explanation for the presence of a substantial fraction of GlyR-enriched clusters at a distance from GlyT2+ profiles is that some of them may be extrasynaptic or intracellular clusters (Hanus et al., 2004), as suggested by the fact that the staining of GlyR-enriched clusters located at >0.6 μm from a GlyT2+ varicosity was significantly lower than that of apposed clusters (Fig. 4*D*,*E*). However, the presence of GlyR-enriched clusters at synapses that do not face glycinergic interneurons cannot be excluded. Overall, these data indicate that GlyR-enriched clusters are preferentially involved in inhibitory transmission at the synapses of CN interneurons, whereas GABAR-enriched clusters are located at PC synapses.

The abundance of GABAR-enriched clusters, particularly on the somata of principal neurons, fits well with the known distribution of PC synapses (De Zeeuw and Berrebi, 1995). To confirm this hypothesis, we performed pan-GlyR/GABAR-γ2 costaining in *L7-ChR2-YFP* transgenic mice (Chaumont et al., 2013) in which expression of ChR2 and YFP was under the control of the Purkinje-specific L7 promoter (Fig. 5*F*). GABAR-enriched clusters faced L7-ChR2-YFP+ terminals on the somata and in the neuropil, but the density of L7-YFP staining prevented proper segmentation of the L7-ChR2-YFP+ terminals and distance quantification. In contrast, GlyR-enriched clusters were generally found between L7-ChR2-YFP+ profiles decorating the somata

and proximal dendrites, confirming that they are in apposition to another presynaptic element.

GABAR-enriched clusters and the majority of GlyR-enriched clusters are located on the membranes of principal CN neurons

The CN contain three main cell types: principal projection neurons, nucleo-olivary neurons, and inhibitory interneurons. Whereas PCs target all three cell types (De Zeeuw and Berrebi, 1995; Teune et al., 1998), the targets of local interneurons are not well characterized (Chen and Hillman, 1993; De Zeeuw and Berrebi, 1995). We thus investigated the postsynaptic localization of GlyR-containing postsynaptic clusters. In line 18 *Thy1-ChR2-YFP* mice (Wang et al., 2007), YFP is a specific marker of principal cells as opposed to local interneurons or nucleo-olivary neurons. All large CN projection neurons, characterized by their somatic VGluT2 immunoreactivity (data not shown), but none of the small cells, exhibited YFP staining at their plasma membrane. We performed costaining for pan-GlyR and GABAR-γ2 in *Thy1-ChR2-YFP* mouse (Fig. 5*G*) and classified all clusters as described previously. The total YFP signal located under each cluster in original and flipped YFP stacks was integrated to evaluate colocalization (Figs. 1, 4*H*,*I*; see Materials and Methods). Virtually all GABAR-enriched clusters (at least 88%; Fig. 5*H*) were found colocalized with YFP, indicating that they are located on principal neurons. A majority of GlyR-enriched clusters (59%) were also colocalized with YFP staining and thus located on principal cells (Fig. 5*I*). The remaining 41% of GlyR-enriched clusters may be located on other cell types or intracellularly in principal cells. We conclude that interneuronal synapses onto CN principal cells should differ from PC synapses by the presence of a large glycinergic component.

Evidence for a small glycinergic component at PC–CN neuron synapses

PC IPSCs recorded in CN principal neurons are generally considered to be purely GABAergic (Obata, 1969; Curtis et al., 1970; De Zeeuw and Berrebi, 1995). We looked for electrophysiological evidence of glycinergic transmission at PC-to-principal CN neuron synapses. CN principal neurons were recorded in whole-cell voltage-clamp configuration in *Thy1-CFP* mice (aged P30–P60) and axons of PCs were electrically stimulated in the white matter surrounding the CN, which is devoid of interneuron axons. Large synaptic currents were evoked (mean, 1108.4 ± 782.1 pA/15.8 ± 11.2 nS, $n = 20$ cells) with a fast decay time course (2.7 ± 0.7 ms, $n = 16$ cells; Telgkamp et al., 2004; Pugh and Raman, 2005; Fig. 6*A*). Application of strychnine at the selective concentration of 300 nM blocked 12.3 ± 7.8% of the peak current (control, 1347.7 ± 965.5 pA/19.3 ± 13.8 nS; strychnine 300 nM, 1198.7 ± 876.2 pA/17.1 ± 12.5 nS, $n = 10$ cells). Subsequent application of 1 μM strychnine produced a further block of the peak current, attaining a total of 39.1 ± 12.0% (888.9 ± 718.0 pA/12.7 ± 10.3 nS $n = 8$ cells; Wilcoxon test paired, $n = 8$ paired cells, $p = 0.0078$) of the initial peak value (Fig. 6*B*). Finally, addition of 300 nM gabazine blocked 84.5 ± 6.5% of the isolated GABAergic component remaining in 1 μM strychnine ($n = 7$ cells; Fig. 6*B*). The large additional block by 1 μM strychnine over 300 nM strychnine is most likely due in part to the well known antagonistic effect of strychnine on GABA receptors (Yakushiji et al., 1987; Jonas et al., 1998), casting doubts on the true size of the glycinergic component at PC synapses.

To provide better quantitative evidence, we applied a two-step strategy. We first blocked 81.4 ± 8.6% (control, 869.1 ± 481.6 pA/12.4 ± 6.9 nS; gabazine 300 nM, 151.8 ± 88.5 pA/2.2 ± 1.3 nS, $n = 10$ cells) of the synaptic current with a selective concentration of gabazine (SR-95531, 300 nM), an antagonist of $GABA_AR$ (Hamann et al., 1988; Fig. 6*C*). We then assessed whether strychnine had an enhanced action on the remaining component of synaptic current, putatively enriched in glycinergic conductance. We found the block of the gabazine-resistant current to be 27.2 ± 11.6% (111.4 ± 73.1 pA/1.6 ± 1.0 nS, $n = 6$ cells) and 48.4 ± 14.3% (83.4 ± 57.1 pA/1.2 ± 0.8 nS, $n = 8$ cells) for 300 nM and 1 μM strychnine, respectively (Wilcoxon test, $p = 0.019$; Fig. 6*D*,*E*). This is 14.9% (Wilcoxon test $p = 0.02$) and 9.3% (Wilcoxon test $p = 0.16$) more than before gabazine application. The synaptic component blocked by 300 nM strychnine after application of gabazine corresponded to 3.77 ± 1.21% ($n = 6$ cells) of the total control current. This value could be corrected for nonspecific block of GABA receptors to a high estimate of 2.2%, assuming independence of strychnine and gabazine effects on the GABA receptors (see Materials and Methods).

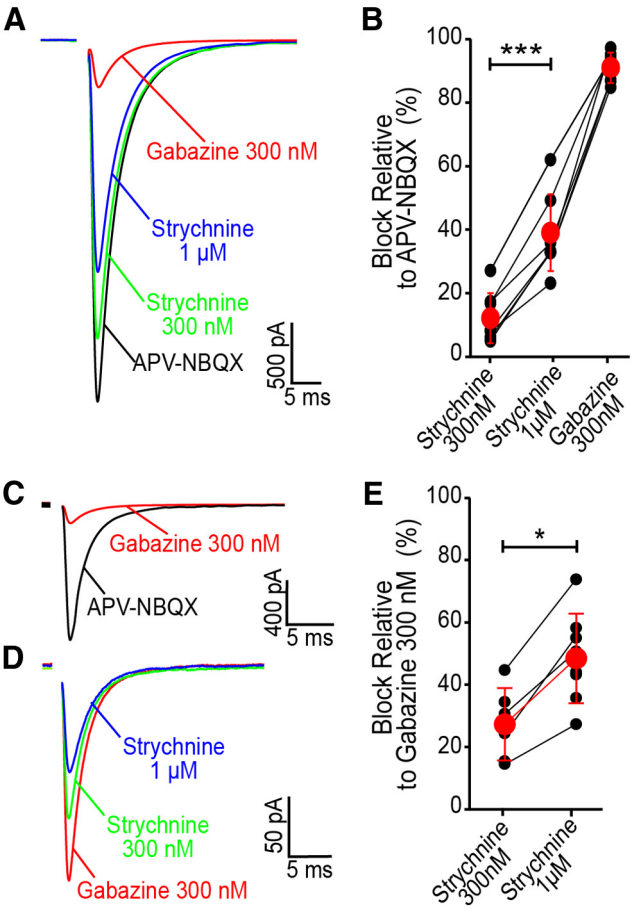

Figure 6. Isolation of a small glycinergic component at Purkinje cell synapses onto principal cells. ***A***, Example of averaged synaptic responses elicited by electrical stimulation of Purkinje cell axons in the white matter surrounding the CN and recorded in CN principal neurons in the presence of blockers of glutamate receptors (50 μM D-APV and 10 μM NBQX). Strychnine (300 nM, 1 μM) and gabazine (300 nM) were successively applied in the bath, resulting in reduction of the peak amplitude. ***B***, Percentage of block by strychnine 300 nM and 1 μM and by gabazine 300 nM relative to the initial response amplitude ($n = 10$, 8, and 7 cells, respectively). ***C***, Application of gabazine 300 nM reduced the peak amplitude by 81.4 ± 8.6% ($n = 10$ cells) and was used to enrich the responses in glycinergic component by increasing the glycinergic fraction in the remaining component. ***D***, ***E***, Block of the remaining current by subsequent application of 300 nM and 1 μM strychnine ($n = 6$ and 8 cells, respectively).

Optogenetic activation of CN interneurons elicits mixed inhibitory synaptic responses in principal neurons

We then investigated the contribution of glycinergic transmission at interneuron-to-principal cell synapses. The properties of this connection are completely unknown because interneurons cannot be excited specifically by extracellular electrodes. We thus used an optogenetic approach. *GlyT2-Cre* mice (1 month old) were injected into the CN with an adeno-associated virus encoding a flexed channelrhodopsin 2 (ChR2) and YFP reporter construct. Three weeks after injection, YFP was expressed specifically in GlyT2-expressing cells of the infected area (Fig. 7*A*,*B*). CN principal neurons from the infected area were recorded in the whole-cell voltage-clamp configuration, whereas interneurons were stimulated by 1 ms illumination of the whole field of view with blue light from a LED at 470 nm (intensities between 0.3 and 4 mW/mm^2). Optogenetic stimulations elicited synaptic currents in principal neurons (Fig. 7*B*,*C*,*E*) with variable efficacy. Maximal intensity illumination failed to evoke any IPSCs in 48.3% of the cells recorded (28 of 58). In the remaining cells, the average peak amplitude of the IPSCs varied between 26 and 785 pA (mean, 145.02 ± 152.24 pA/2.1 ± 2.1 nS, $n = 43$ cells; Fig. 7*B*). As in the *GlyT2-eGFP* mouse, only 40% of GlyT2-positive elements at best are colabeled for YFP in the *GlyT2-Cre* mouse injected with ChR2-YFP viruses at a postnatal stage (data not shown). This partial infection of the glycinergic interneuronal population, as well as variable preservation of connections in the slices, may explain the heterogeneity of the evoked synaptic responses. A paired-pulse ratio (PPR) of 1.00 ± 0.16 ($n = 14$ cells) was measured for a 100 ms interval between optical stimulations, slighter lower than the PPR at PC synapses (1.09 ± 0.13, $n = 14$; Wilcoxon test $p = 0.021$), suggesting similar release probability at the two synapses. The decay times of the synaptic events at these two synapses were not significantly different (Purkinje cell synapse, 2.67 ± 0.66 ms, $n = 16$ cells; interneuronal synapse, 3.07 ± 0.99 ms, $n = 15$ cells; Wilcoxon test $p = 0.2316$).

Strychnine and gabazine were applied to quantify the contribution of glycinergic transmission at the interneuron-to-principal cell synapse. Application of 300 nM strychnine blocked 34.7 ± 14.9% of the initial amplitude (control, 154.2 ± 92.3 pA/2.2 ± 1.3 nS; strychnine 300 nM, 97.3 ± 59.6 pA/1.4 ± 0.9 nS, $n = 13$ cells; Fig. 7*C*,*D*), significantly more than at the PC synapse (Wilcoxon test, $p = 0.0025$). The percentage block by strychnine was highly variable between cells (minimum = 5.8%, maximum = 52.7%). At a concentration of 1 μM, strychnine produced a larger block of 51.1 ± 20.5 % (73.8 ± 48.6 pA/1.1 ± 0.7 nS; $n = 14$ cells; Wilcoxon test paired, $n = 10$ cells paired, $p = 0.0019$; Fig. 7*C*,*D*), consistent with a nonspecific action on GABARs. Addition of 300 nM gabazine blocked virtually all the remaining current (94.2 ± 4.9% of the remaining value, 4.3 ± 3.6 pA/0.06 ± 0.05 nS, $n = 7$ cells; Fig. 7*C*,*D*). This is significantly different from the block of the isolated GABA component at the Purkinje cell synapses (84.5 ± 6.5%, $n = 7$ cells; Wilcoxon test, $p = 0.0297$), consistent with a difference in the molecular identity of GABAR present at the two synapses, as suggested by immunohistochemistry.

We applied the same two-step strategy as previously described at the Purkinje cell-to-principal neuron synapse, to provide a reliable estimate of the glycinergic and GABAergic components at the interneuronal synapse. Application of 300 nM gabazine blocked 76.7 ± 10.9% of the initial amplitude (control, 161.6 ± 169.6 pA/2.3 ± 2.4 nS; gabazine 300 nM, 29.6 ± 18.5 pA/0.42 ± 0.27 nS, $n = 11$ cells; (Fig. 7*E*,*F*). Following application of strychnine 300 nM, the gabazine-resistant current was blocked by 56.3 ± 19.9% (14.5 ± 14.5 pA/0.21 ± 0.21 nS, $n = 10$ cells), significantly more than at the Purkinje cell synapse (Wilcoxon test $p = 0.01099$, Purkinje cells synapse, 27.2 ± 11.6%, $n = 6$ cells). This represented a fraction of the original current of 14.7 ± 8.2% ($n = 11$ cells), significantly higher than that at the Purkinje cell synapse (3.8 ± 1.2%, $n = 6$ cells, Wilcoxon test $p = 0.02731$; Fig. 7*G*). Correction for nonspecific block of the GABA component yielded an estimated glycinergic component of 13.6%.

These results provide the first evidence for functional inhibitory neurotransmission at interneuronal synapses onto principal cells of the CN. They establish the presence of a large glycinergic component, as a distinctive feature of interneuron IPSCs in principal cells.

Discussion

Inhibitory glycinergic neurons in the CN

We examined the function of CN glycinergic interneurons using the *GlyT2-eGFP* and *GlyT2-cre* transgenic models. Glycinergic CN neurons are specifically stained in adult *GlyT2-eGFP* animals, where GFP+ neurons form a population distinct from retrogradely labeled nucleo-olivary cells (Fig. 3) and morphologically different from principal cells. Only 40% of the glycinergic neurons express GFP in adult *GlyT2-eGFP* mice, as confirmed by the incomplete colocalization with GFP of GlyT2-immunoreactive profiles (Fig. 2) and of GABA-immunoreactive cell bodies (Fig. 3), and by the partial apposition of GFP with GlyR-enriched clusters (Fig. 5). Taking this mosaic expression into account, the total number of glycinergic neurons in the interposed and lateral CN can be estimated to 3200 bilaterally, similar to the 4000 neurons positive for GABA and glycine but lower than the 8600 glycine-only somata found by Bäurle and Grüsser-Cornehls (1997). Mild accumulation of glycine in glia through the GlyT1 transporter could explain the numerous glycine-only somata in that study. Finally, interneurons account for approximately half of the 10,000 small neurons found by Heckroth (1994) in the mouse CN, the other half being nucleo-olivary cells.

Although complete staining of the glycinergic population can be obtained in a *GlyT2-cre* model, when the cre recombinase is allowed to act on reporter constructs during the whole development (Fig. 2), aspecific expression of the marker extends to some vermal Purkinje cells and to a subpopulation of nucleo-olivary cells (Fig. 2). This pattern of expression might also be present in the young *GlyT2-eGFP* animals (which were generated using the same bacterial artificial chromosome), as indicated by the weak residual GFP staining in some nucleo-olivary cells at 2 months (data not shown). This lack of specificity in young *GlyT2-eGFP* mice might explain why two types of GFP+ cells were distinguished on electrophysiological criteria at P20–P27 (Uusisaari and Knöpfel, 2010). The first type fires spontaneously and is functionally similar to small GAD67-GFP-positive nucleo-olivary cells (Uusisaari et al., 2007; Uusisaari and Knöpfel, 2008). A second population of larger GFP+ neurons was spontaneously inactive, in agreement with the rare occurrence of spontaneous glycinergic events in principal cells (Chen and Hillman, 1993; Pedroarena and Kamphausen, 2008; this study). These neurons displayed a local axonal plexus, as described in this study, and may also project toward the cortex (Uusisaari and Knöpfel, 2010). Finally, these neurons fired at high frequency in response to large current injections (Uusisaari and Knöpfel, 2010), reminiscent of the bursts of high-frequency IPSCs we recorded in principal CN neurons in response to saturating optogenetic stimulations. We conclude that glycinergic CN neurons constitute a separate class of medium-sized spontaneously inac-

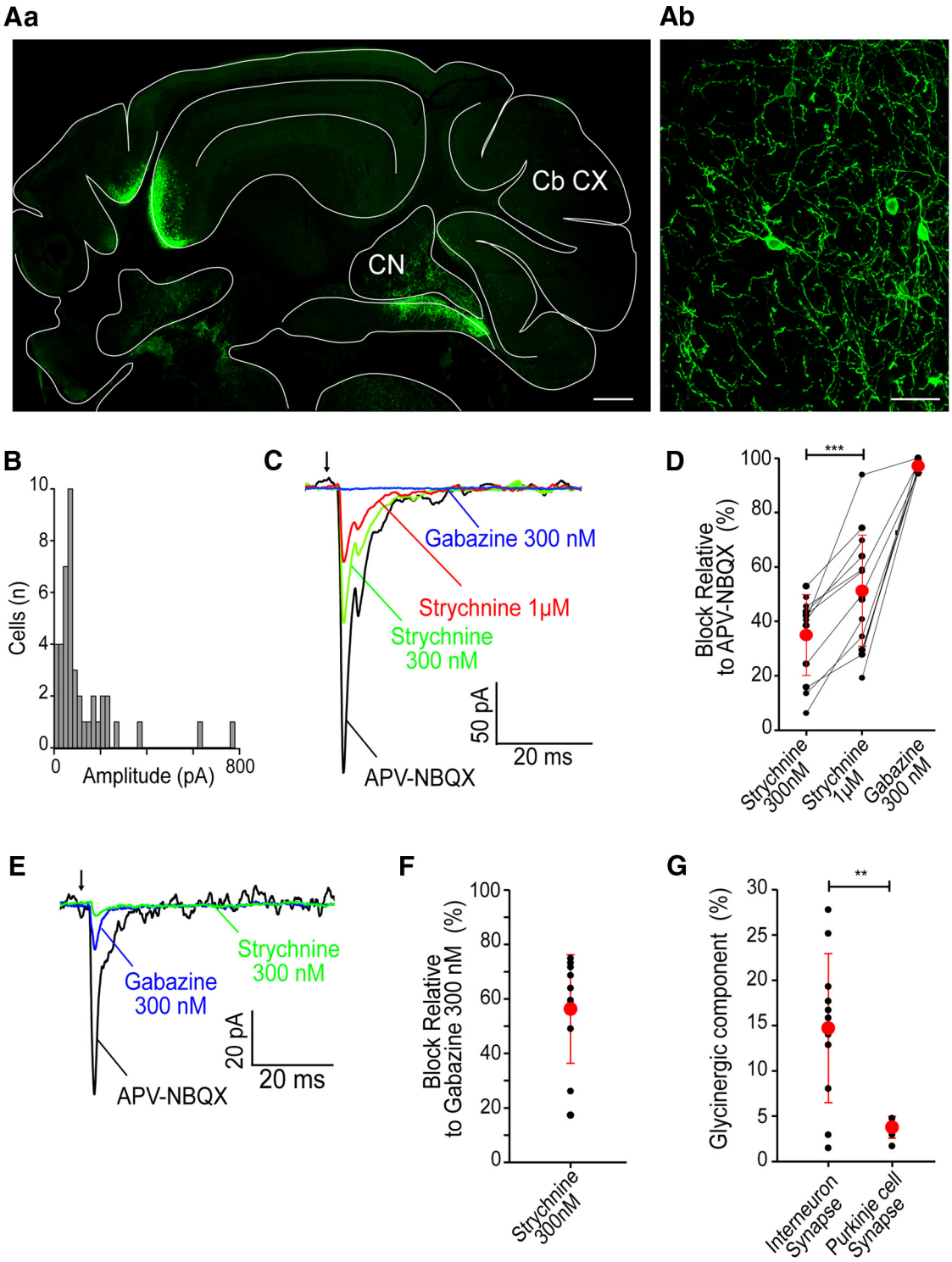

Figure 7. Mixed inhibition at CN interneuron synapses on principal cells. ***Aa***, Coronal slice of cerebellum from a *GlyT2-Cre* mouse injected bilaterally into the CN with a flexed virus expressing ChR2-YFP. ***Ab***, After 3 weeks of infection, GlyT2-expressing neurons exhibit ChR2-YFP staining at their membrane. ***B***, Histogram of the peak amplitude of the synaptic currents evoked by 1 ms optogenetic stimulation of the CN glycinergic neurons and recorded in CN principal neurons ($n = 43$ cells). ***C***, Example of averaged synaptic currents recorded in the presence of blockers of excitation (50 μM D-APV and 10 μM NBQX) and of their block by successive application of strychnine and gabazine. ***D***, Summary of the sensitivity of the synaptic currents to strychnine 300 nM and 1 μM ($n =$ 13 and 14 cells, respectively; Wilcoxon test paired, $n = 10$ paired cells, $p = 0.0019$) and gabazine 300 nM (97.0 $\pm$ 2.3% block relative to initial response amplitude, $n = 7$ cells). ***E***, Example of average responses (in the presence of 50 μM D-APV and 10 μM NBQX) when reverse pharmacology was performed. Gabazine 300 nM was applied before 300 nM strychnine and blocked 76.7 $\pm$ 10.9% of the control amplitude ($n = 11$ cells). ***F***, Percentage of block by strychnine 300 nM relative to the remaining current after application of 300 nM gabazine ($n = 11$ cells). ***G***, Glycinergic component of the initial response was assessed by the following formula: [(Amplitude after 300 nM gabazine $-$ Amplitude after 300 nM gabazine and 300 nM strychnine)/Amplitude of the initial response]. This glycinergic component is higher at the interneuronal synapse than at the Purkinje cell synapse ($n = 11$ and 6 cells, respectively; Wilcoxon test $p = 0.02731$). Scale bars: ***Aa***, 500 μm; ***Ab***, 50 μm. Cb Cx, Cerebellar cortex.

tive neurons, which may account for half of the non-principal neurons in the CN.

Some aspects of the microcircuit organization of glycinergic CN neurons appeared as incidental observations in previous studies (Chen and Hillman, 1993; De Zeeuw and Berrebi, 1995; Pedroarena and Kamphausen, 2008). We show here that glycinergic boutons face GlyR-enriched synapses (Figs. 3, 4) which account for ~4% of the number of inhibitory clusters on principal neurons. The existence of an equivalent population of GlyR-enriched clusters that is located neither on principal cells (Fig. 5) nor on the somata or primary dendrites of GlyT2-GFP interneurons confirms the early observation that glycinergic terminals contact GABA-containing neurons (De Zeeuw and Berrebi, 1995), most likely nucleo-olivary GABAergic cells.

Mixed GABA-glycine transmission in the CN

Mixed release of GABA and glycine is a common mode of inhibitory transmission in the cerebellar cortex (Dumoulin et al., 2001; Rousseau et al., 2012). In the CN, GlyT2-positive neurons express GAD67 (Tanaka and Ezure, 2004), as do nucleo-olivary cells (Fredette and Mugnaini, 1991; Tamamaki et al., 2003). Surprisingly, a single functional class of small GFP-positive neurons and a separate class of GFP-negative neurons was described in the CN of *GAD67-GFP* knock-in animals (Uusisaari et al., 2007; Uusisaari and Knöpfel, 2008), suggesting that glycinergic interneurons may not be stained in this transgenic line. We find here that most GlyT2-immunoreactive varicosities are positive for GAD, indicating that glycinergic CN neurons consistently corelease GABA and glycine.

We took advantage of the cell-type specificity of optogenetic stimulations to reveal and characterize the functional synapses between glycinergic interneurons and principal cells in the CN. Light-evoked IPSCs always contained both GABAR-mediated and GlyR-mediated components with an average GlyR contribution of 15% of the amplitude (Fig. 7). This large glycinergic component differentiates interneuron IPSCs from PC IPSCs (Fig. 6), for which <3% of the amplitude is mediated by GlyR, whereas IPSC decay kinetics are similar at both synapses. Paired stimulations gave similar PPRs at interneuronal (Fig. 7) and Purkinje synapses (Telgkamp et al., 2004), but longer stimulation trains should be tested. Spillover between release sites onto multiple receptor clusters (Telgkamp et al., 2004) accounts for sustained high-frequency transmission at large Purkinje cell boutons. The sensitivity of GlyR to glycine spillover and temporal summation (Beato et al., 2007; Balakrishnan et al., 2009) could favor GlyR currents during high-frequency activity at interneuronal synapses.

The presence of small aggregates of GlyR α1 subunits at PC synapses onto principal neurons and of a small glycinergic component of the IPSCs is surprising, as PCs are not known to release glycine (Tanaka and Ezure, 2004). GABA can activate GlyR with low efficacy (De Saint Jan et al., 2001; Legendre, 2001), evoking fast decaying GlyR-IPSCs (Lu et al., 2008) with kinetics similar to those of the PC IPSCs (Fig. 6; Person and Raman, 2012a). The functional role of this small glycinergic component is elusive, and the presence of GlyR at GABAergic synapses may result from structural entrapment during synapse formation (Dumoulin et al., 2000; Muller et al., 2004), as both GABAR (Sassoè-Pognetto et al., 2000) and GlyR (Meyer et al., 1995) bind to the same postsynaptic scaffolding protein, gephyrin.

At interneuronal synapses, GlyR-enriched clusters contain the α1 subunit of the glycine receptor (Fig. 4; Malosio et al., 1991), most likely associated with the β subunit, which is expressed in the CN (Weltzien et al., 2012) and is responsible for the clustering of GlyR at synapses (Kneussel and Betz, 2000). GlyR-enriched clusters are virtually devoid of the α1 and γ2 GABAR subunits, the most abundant subunits in the CN (Persohn et al., 1992; Gambarana et al., 1993), found at PC synapses onto principal cells (Fig. 4). However, pharmacological analysis of the interneuron IPSCs demonstrates the presence of functional GABAR (Fig. 7). Although α3-GABAR subunits are expressed in the CN, they appear to mediate slow IPSCs at PC synapses onto GABAergic cells (Uusisaari and Knöpfel, 2008), different from the fast optically evoked IPSCs in principal cells. It is thus likely that other GABAR subunits, such as α5 or γ1 (Pirker et al., 2000; Hörtnagl et al., 2013), are involved at interneuronal synapses onto principal cells.

Functional impact of interneuronal inhibition in the CN

The average IPSC conductance evoked by optogenetic stimulations (2 nS; Fig. 7) gives the strength of the interneuronal input to principal neurons. Because 40% of interneurons at best express ChR2 upon viral infection in *GlyT2-Cre* animals, the average interneuronal synaptic conductance should exceed 5 nS, ~4% of the average conductance evoked by maximal electrical stimulation of PC axons in the slice (Person and Raman, 2012a). Our optogenetic stimulations and the electrical stimulations of Person and Raman (2012b) represent a large underestimate of the total inputs, as many synapses will not be recruited due to failed stimulation or disrupted connectivity in slices. However, their ratio is in excellent agreement with previous electron microscopy estimates of glycine-containing synapses in the CN (2% of all contacts; De Zeeuw and Berrebi, 1995) and with our immunohistochemical staining (5% of contacts on principal cells).

Two types of spontaneous IPSCs/IPSPs have been recorded from CN principal neurons *in vivo* (Bengtsson et al., 2011; Witter et al., 2013): a barrage of low-amplitude and high-frequency synaptic events reflecting the spontaneous firing of presynaptic PCs (Person and Raman, 2012a), and giant low-frequency IPSC/Ps. Giant IPSC/Ps have been proposed to result from the synchronization of PCs by climbing fibers (Bengtsson et al., 2011; Person and Raman, 2012b; Witter et al., 2013). Indeed, large IPSCs are readily evoked during tactile stimulations of the cutaneous climbing fiber receptive field (Bengtsson and Jörntell, 2014) and by electrical stimulations of the inferior olive (Hoebeek et al., 2010; Bengtsson et al., 2011), driving powerful rebound firing of the CN cells which induces plasticity at CN synapses (Aizenman et al., 1998; Pugh and Raman, 2006). Surprisingly, direct synchronization of PCs by stimulation of the cerebellar cortex did not produce a robust rebound firing of CN cells (Hoebeek et al., 2010; Person and Raman, 2012a). The difference in the effects of olivary and cortical stimulations has been tentatively explained by assuming that inferior olive activity recruits functionally significant sparse patterns of PCs (Welsh et al., 1995; Ozden et al., 2009, 2012; Schultz et al., 2009). Alternatively, one should consider the possibility that giant IPSC/Ps recorded from CN principal cells arise from the synchronous activity of several CN interneurons and not from PC synchronization.

References

Aizenman CD, Manis PB, Linden DJ (1998) Polarity of long-term synaptic gain change is related to postsynaptic spike firing at a cerebellar inhibitory synapse. Neuron 21:827–835. CrossRef Medline

Araki T, Sato M, Kiyama H, Manabe Y, Tohyama M (1992) Localization of GABAA-receptor gamma 2-subunit mRNA-containing neurons in the rat central nervous system. Neuroscience 47:45–61. CrossRef Medline

Bagnall MW, Zingg B, Sakatos A, Moghadam SH, Zeilhofer HU, du Lac S

(2009) Glycinergic projection neurons of the cerebellum. J Neurosci 29: 10104–10110. CrossRef Medline

Balakrishnan V, Kuo SP, Roberts PD, Trussell LO (2009) Slow glycinergic transmission mediated by transmitter pooling. Nat Neurosci 12:286–294. CrossRef Medline

Bäurle J, Grüsser-Cornehls U (1997) Differential number of glycine- and GABA-immunopositive neurons and terminals in the deep cerebellar nuclei of normal and Purkinje cell degeneration mutant mice. J Comp Neurol 382:443–458. CrossRef Medline

Beato M, Burzomato V, Sivilotti LG (2007) The kinetics of inhibition of rat recombinant heteromeric alpha1beta glycine receptors by the low-affinity antagonist SR-95531. J Physiol 580:171–179. CrossRef Medline

Bengtsson F, Jörntell H (2014) Specific relationship between excitatory inputs and climbing fiber receptive fields in deep cerebellar nuclear neurons. PLoS One 9:e84616. CrossRef Medline

Bengtsson F, Ekerot CF, Jörntell H (2011) In vivo analysis of inhibitory synaptic inputs and rebounds in deep cerebellar nuclear neurons. PLoS One 6:e18822. CrossRef Medline

Best AR, Regehr WG (2009) Inhibitory regulation of electrically coupled neurons in the inferior olive is mediated by asynchronous release of GABA. Neuron 62:555–565. CrossRef Medline

Bolte S, Cordelières FP (2006) A guided tour into subcellular colocalization analysis in light microscopy. J Microsc 224:213–232. CrossRef Medline

Chaumont J, Guyon N, Valera AM, Dugué GP, Popa D, Marcaggi P, Gautheron V, Reibel-Foisset S, Dieudonné S, Stephan A, Barrot M, Cassel JC, Dupont JL, Doussau F, Poulain B, Selimi F, Léna C, Isope P (2013) Clusters of cerebellar Purkinje cells control their afferent climbing fiber discharge. Proc Natl Acad Sci U S A 110:16223–16228. CrossRef Medline

Chen S, Hillman DE (1993) Colocalization of neurotransmitters in the deep cerebellar nuclei. J Neurocytol 22:81–91. CrossRef Medline

Chen X, Kovalchuk Y, Adelsberger H, Henning HA, Sausbier M, Wietzorrek G, Ruth P, Yarom Y, Konnerth A (2010) Disruption of the olivocerebellar circuit by Purkinje neuron-specific ablation of BK channels. Proc Natl Acad Sci U S A 107:12323–12328. CrossRef Medline

Curtis DR, Duggan AW, Felix D (1970) GABA and inhibition of Deiters' neurones. Brain Res 23:117–120. CrossRef Medline

De Saint Jan D, David-Watine B, Korn H, Bregestovski P (2001) Activation of human alpha1 and alpha2 homomeric glycine receptors by taurine and GABA. J Physiol 535:741–755. CrossRef Medline

De Zeeuw CI, Berrebi AS (1995) Postsynaptic targets of Purkinje cell terminals in the cerebellar and vestibular nuclei of the rat. Eur J Neurosci 7:2322–2333. CrossRef Medline

De Zeeuw CI, Van Alphen AM, Hawkins RK, Ruigrok TJ (1997) Climbing fibre collaterals contact neurons in the cerebellar nuclei that provide a GABAergic feedback to the inferior olive. Neuroscience 80:981–986. CrossRef Medline

Dougherty R (2005) Extensions of DAMAS and benefits and limitations of deconvolution in beamforming. Presented at the 11th AIAA/CEAS Aeroacoustics Conference, May 23–25, Monterey, CA.

Dumoulin A, Lévi S, Riveau B, Gasnier B, Triller A (2000) Formation of mixed glycine and GABAergic synapses in cultured spinal cord neurons. Eur J Neurosci 12:3883–3892. CrossRef Medline

Dumoulin A, Triller A, Dieudonné S (2001) IPSC kinetics at identified GABAergic and mixed GABAergic and glycinergic synapses onto cerebellar Golgi cells. J Neurosci 21:6045–6057. Medline

Feng G, Mellor RH, Bernstein M, Keller-Peck C, Nguyen QT, Wallace M, Nerbonne JM, Lichtman JW, Sanes JR (2000) Imaging neuronal subsets in transgenic mice expressing multiple spectral variants of GFP. Neuron 28:41–51. CrossRef Medline

Fredette BJ, Mugnaini E (1991) The GABAergic cerebello-olivary projection in the rat. Anat Embryol (Berl) 184:225–243. CrossRef Medline

Gambarana C, Loria CJ, Siegel RE (1993) GABAA receptor messenger RNA expression in the deep cerebellar nuclei of Purkinje cell degeneration mutants is maintained following the loss of innervating Purkinje neurons. Neuroscience 52:63–71. CrossRef Medline

Hamann M, Desarmenien M, Desaulles E, Bader MF, Feltz P (1988) Quantitative evaluation of the properties of a pyridazinyl GABA derivative (SR 95531) as a GABAA competitive antagonist. An electrophysiological approach. Brain Res 442:287–296. CrossRef Medline

Hanus C, Vannier C, Triller A (2004) Intracellular association of glycine receptor with gephyrin increases its plasma membrane accumulation rate. J Neurosci 24:1119–1128. CrossRef Medline

Heckroth JA (1994) Quantitative morphological analysis of the cerebellar nuclei in normal and lurcher mutant mice. I. Morphology and cell number. J Comp Neurol 343:173–182. CrossRef Medline

Hoebeek FE, Witter L, Ruigrok TJ, De Zeeuw CI (2010) Differential olivocerebellar cortical control of rebound activity in the cerebellar nuclei. Proc Natl Acad Sci U S A 107:8410–8415. CrossRef Medline

Hörtnagl H, Tasan RO, Wieselthaler A, Kirchmair E, Sieghart W, Sperk G (2013) Patterns of mRNA and protein expression for 12 GABAA receptor subunits in the mouse brain. Neuroscience 236:345–372. CrossRef Medline

Houck BD, Person AL (2014) Cerebellar loops: a review of the nucleocortical pathway. Cerebellum 13:378–385. CrossRef Medline

Isope P, Barbour B (2002) Properties of unitary granule cell–>Purkinje cell synapses in adult rat cerebellar slices. J Neurosci 22:9668–9678. Medline

Ito M, Yoshida M, Obata K, Kawai N, Udo M (1970) Inhibitory control of intracerebellar nuclei by the purkinje cell axons. Exp Brain Res 10:64–80. CrossRef Medline

Jonas P, Bischofberger J, Sandkühler J (1998) Corelease of two fast neurotransmitters at a central synapse. Science 281:419–424. CrossRef Medline

Kawa K (2003) Glycine receptors and glycinergic synaptic transmission in the deep cerebellar nuclei of the rat: a patch-clamp study. J Neurophysiol 90:3490–3500. CrossRef Medline

Kneussel M, Betz H (2000) Clustering of inhibitory neurotransmitter receptors at developing postsynaptic sites: the membrane activation model. Trends Neurosci 23:429–435. CrossRef Medline

Kravitz AV, Freeze BS, Parker PR, Kay K, Thwin MT, Deisseroth K, Kreitzer AC (2010) Regulation of parkinsonian motor behaviours by optogenetic control of basal ganglia circuitry. Nature 466:622–626. CrossRef Medline

Legendre P (2001) The glycinergic inhibitory synapse. Cell Mol Life Sci 58: 760–793. CrossRef Medline

Lu T, Rubio ME, Trussell LO (2008) Glycinergic transmission shaped by the corelease of GABA in a mammalian auditory synapse. Neuron 57:524–535. CrossRef Medline

Machado P, Rostaing P, Guigonis JM, Renner M, Dumoulin A, Samson M, Vannier C, Triller A (2011) Heat shock cognate protein 70 regulates gephyrin clustering. J Neurosci 31:3–14. CrossRef Medline

Malosio ML, Marquèze-Pouey B, Kuhse J, Betz H (1991) Widespread expression of glycine receptor subunit mRNAs in the adult and developing rat brain. EMBO J 10:2401–2409. Medline

Matsushita M, Iwahori N (1971) Structural organization of the interpositus and the dentate nuclei. Brain Res 35:17–36. CrossRef Medline

McCrea RA, Bishop GA, Kitai ST (1978) Morphological and electrophysiological characteristics of projection neurons in the nucleus interpositus of the cat cerebellum. J Comp Neurol 181:397–419. CrossRef Medline

Medina JF, Nores WL, Ohyama T, Mauk MD (2000) Mechanisms of cerebellar learning suggested by eyelid conditioning. Curr Opin Neurobiol 10:717–724. CrossRef Medline

Meyer G, Kirsch J, Betz H, Langosch D (1995) Identification of a gephyrin binding motif on the glycine receptor beta subunit. Neuron 15:563–572. CrossRef Medline

Miles FA, Lisberger SG (1981) Plasticity in the vestibulo-ocular reflex: a new hypothesis. Annu Rev Neurosci 4:273–299. CrossRef Medline

Muller E, Triller A, Legendre P (2004) Glycine receptors and GABA receptor alpha 1 and gamma 2 subunits during the development of mouse hypoglossal nucleus. Eur J Neurosci 20:3286–3300. CrossRef Medline

Muzumdar MD, Tasic B, Miyamichi K, Li L, Luo L (2007) A global double-fluorescent Cre reporter mouse. Genesis 45:593–605. CrossRef Medline

Obata K (1969) Gamma-aminobutyric acid in Purkinje cells and motoneurones. Experientia 25:1283. CrossRef Medline

Ozden I, Sullivan MR, Lee HM, Wang SS (2009) Reliable coding emerges from coactivation of climbing fibers in microbands of cerebellar Purkinje neurons. J Neurosci 29:10463–10473. CrossRef Medline

Ozden I, Dombeck DA, Hoogland TM, Tank DW, Wang SS (2012) Widespread state-dependent shifts in cerebellar activity in locomoting mice. PLoS One 7:e42650. CrossRef Medline

Pedroarena CM, Kamphausen S (2008) Glycinergic synaptic currents in the deep cerebellar nuclei. Neuropharmacology 54:784–795. CrossRef Medline

Persohn E, Malherbe P, Richards JG (1992) Comparative molecular neuro-

anatomy of cloned GABAA receptor subunits in the rat CNS. J Comp Neurol 326:193–216. CrossRef Medline

Person AL, Raman IM (2012a) Purkinje neuron synchrony elicits time-locked spiking in the cerebellar nuclei. Nature 481:502–505. CrossRef Medline

Person AL, Raman IM (2012b) Synchrony and neural coding in cerebellar circuits. Front Neural Circuits 6:97. CrossRef Medline

Pirker S, Schwarzer C, Wieselthaler A, Sieghart W, Sperk G (2000) GABA(A) receptors: immunocytochemical distribution of 13 subunits in the adult rat brain. Neuroscience 101:815–850. CrossRef Medline

Pugh JR, Raman IM (2005) GABAA receptor kinetics in the cerebellar nuclei: evidence for detection of transmitter from distant release sites. Biophys J 88:1740–1754. CrossRef Medline

Pugh JR, Raman IM (2006) Potentiation of mossy fiber EPSCs in the cerebellar nuclei by NMDA receptor activation followed by postinhibitory rebound current. Neuron 51:113–123. CrossRef Medline

Rampon C, Luppi PH, Fort P, Peyron C, Jouvet M (1996) Distribution of glycine-immunoreactive cell bodies and fibers in the rat brain. Neuroscience 75:737–755. CrossRef Medline

Rousseau CV, Dugué GP, Dumoulin A, Mugnaini E, Dieudonné S, Diana MA (2012) Mixed inhibitory synaptic balance correlates with glutamatergic synaptic phenotype in cerebellar unipolar brush cells. J Neurosci 32:4632–4644. CrossRef Medline

Sassoè-Pognetto M, Panzanelli P, Sieghart W, Fritschy JM (2000) Colocalization of multiple GABA(A) receptor subtypes with gephyrin at postsynaptic sites. J Comp Neurol 420:481–498. CrossRef Medline

Schindelin J, Arganda-Carreras I, Frise E, Kaynig V, Longair M, Pietzsch T, Preibisch S, Rueden C, Saalfeld S, Schmid B, Tinevez JY, White DJ, Hartenstein V, Eliceiri K, Tomancak P, Cardona A (2012) Fiji: an open-source platform for biological-image analysis. Nat Methods 9:676–682. CrossRef Medline

Schultz SR, Kitamura K, Post-Uiterweer A, Krupic J, Häusser M (2009) Spatial pattern coding of sensory information by climbing fiber-evoked calcium signals in networks of neighboring cerebellar Purkinje cells. J Neurosci 29:8005–8015. CrossRef Medline

Tamamaki N, Yanagawa Y, Tomioka R, Miyazaki J, Obata K, Kaneko T (2003) Green fluorescent protein expression and colocalization with calretinin, parvalbumin, and somatostatin in the GAD67-GFP knock-in mouse. J Comp Neurol 467:60–79. CrossRef Medline

Tanaka I, Ezure K (2004) Overall distribution of GLYT2 mRNA-containing versus GAD67 mRNA-containing neurons and colocalization of both mRNAs in midbrain, pons, and cerebellum in rats. Neurosci Res 49:165–178. CrossRef Medline

Telgkamp P, Padgett DE, Ledoux VA, Woolley CS, Raman IM (2004) Maintenance of high-frequency transmission at purkinje to cerebellar nuclear synapses by spillover from boutons with multiple release sites. Neuron 41:113–126. CrossRef Medline

Teune TM, van der Burg J, de Zeeuw CI, Voogd J, Ruigrok TJ (1998) Single Purkinje cell can innervate multiple classes of projection neurons in the cerebellar nuclei of the rat: a light microscopic and ultrastructural triple-tracer study in the rat. J Comp Neurol 392:164–178. CrossRef Medline

Uusisaari M, Knöpfel T (2008) GABAergic synaptic communication in the GABAergic and non-GABAergic cells in the deep cerebellar nuclei. Neuroscience 156:537–549. CrossRef Medline

Uusisaari M, Knöpfel T (2010) GlyT2+ neurons in the lateral cerebellar nucleus. Cerebellum 9:42–55. CrossRef Medline

Uusisaari MY, Knöpfel T (2012) Diversity of neuronal elements and circuitry in the cerebellar nuclei. Cerebellum 11:420–421. CrossRef Medline

Uusisaari M, Obata K, Knöpfel T (2007) Morphological and electrophysiological properties of GABAergic and non-GABAergic cells in the deep cerebellar nuclei. J Neurophysiol 97:901–911. CrossRef Medline

Wang H, Peca J, Matsuzaki M, Matsuzaki K, Noguchi J, Qiu L, Wang D, Zhang F, Boyden E, Deisseroth K, Kasai H, Hall WC, Feng G, Augustine GJ (2007) High-speed mapping of synaptic connectivity using photostimulation in Channelrhodopsin-2 transgenic mice. Proc Natl Acad Sci U S A 104:8143–8148. CrossRef Medline

Wassef M, Simons J, Tappaz ML, Sotelo C (1986) Non-Purkinje cell GABAergic innervation of the deep cerebellar nuclei: a quantitative immunocytochemical study in C57BL and in Purkinje cell degeneration mutant mice. Brain Res 399:125–135. CrossRef Medline

Welsh JP, Lang EJ, Suglhara I, Llinás R (1995) Dynamic organization of motor control within the olivocerebellar system. Nature 374:453–457. CrossRef Medline

Weltzien F, Puller C, O'Sullivan GA, Paarmann I, Betz H (2012) Distribution of the glycine receptor beta-subunit in the mouse CNS as revealed by a novel monoclonal antibody. J Comp Neurol 520:3962–3981. CrossRef Medline

Witter L, Canto CB, Hoogland TM, de Gruijl JR, De Zeeuw CI (2013) Strength and timing of motor responses mediated by rebound firing in the cerebellar nuclei after Purkinje cell activation. Front Neural Circuits 7:133. CrossRef Medline

Yakushiji T, Tokutomi N, Akaike N, Carpenter DO (1987) Antagonists of GABA responses, studied using internally perfused frog dorsal root ganglion neurons. Neuroscience 22:1123–1133. CrossRef Medline

Zafra F, Aragón C, Olivares L, Danbolt NC, Giménez C, Storm-Mathisen J (1995) Glycine transporters are differentially expressed among CNS cells. J Neurosci 15:3952–3969. Medline

Zeilhofer HU, Studler B, Arabadzisz D, Schweizer C, Ahmadi S, Layh B, Bösl MR, Fritschy JM (2005) Glycinergic neurons expressing enhanced green fluorescent protein in bacterial artificial chromosome transgenic mice. J Comp Neurol 482:123–141. CrossRef Medline

Zheng N, Raman IM (2010) Synaptic inhibition, excitation, and plasticity in neurons of the cerebellar nuclei. Cerebellum 9:56–66. CrossRef Medline